Bacteriophage PR772 X-Ray Free Electron Laser and Cryo-Electron Microscopy Studies

by

Alice Contreras

A Thesis Presented in Partial Fulfillment
of the Requirements for the Degree
Master of Science

Approved July 2019 by the
Graduate Supervisory Committee:

Brenda G. Hogue, Chair
Ian B. Hogue
Dewight Williams

ARIZONA STATE UNIVERSITY

December 2019

ABSTRACT

Structural details about viruses and their components are important for understanding the many steps in a virus lifecycle, including entry into host cells, replication, assembly, and release of progeny virions. X-ray crystallography and electron microscopy, including cryo-EM, have been used extensively for virus structural studies. Recent advances with cryo-EM have significantly advanced the field with near-atomic resolution structures of viruses being achievable. X-ray free-electron lasers (XFELs) are a novel, developing method to solve structures for non-crystalline single particle targets like viruses. Diffraction patterns can be collected directly from particles at room temperature. High quality, homogeneous virus preparations are critical for both cryo-EM and XFEL studies. Thus, optimization of virus growth and sample preparation are important steps in virus structural studies. The work described in this thesis focused on optimization of protocols for growth and purification of bacteriophage PR772 for XFEL and complementary cryo-EM studies. PR772 is one of several model viruses used in the single particle initiative (SPI) experiments at the SLAC National Laboratory Accelerator Laboratory Linac Coherent Light Source (LCLS). SPI is a collaborative international effort that works towards identifying and solving challenges of high-resolution single particle imaging using XFELs. Single particle diffraction snapshots were collected from PR772 particles prepared with optimized protocols. PR772 preparations were also used for cryo-EM imaging, with the goal to obtain a high-resolution structure of the virus. The optimization and characterization employed to assure samples suitable for XFEL and cryo-EM are detailed, along with data collected with both approaches.

DEDICATION

I dedicate this thesis to my great support system, my parents Juan Contreras and Alicia Avalos, and my love Jeremy B. Daley

ACKNOWLEDGMENTS

To begin, I would like to acknowledge the faculty, staff and students of the Biodesign Institute (A, B, and C) for their contributions to a professional, uplifting, and fun work environment. I would like to recognize BioXFEL, whose internship opportunity allowed me to find Dr. Brenda Hogue's lab and attend conferences where I had the opportunity to present my work.

There are several people who have helped make this project a success. I would like to recognize Dewight Williams and the John M. Cowley Center for High Resolution Electron Microscopy of ASU for their help with the electron microscopy and Cryo-EM aspects of this work. I am appreciative of my supervisory committee members, Dr. Ian Hogue and Dewight Williams for their words of encouragement and guidance throughout this process.

A special thank you to my committee chair and mentor Dr. Brenda Hogue. She saw the potential I had even when I had self-doubts. She took a chance by taking me on as her student, a student with average grades and only two years of basic lab experience. She pushed me to better my technique and to not fear the unknown. I would like to acknowledge my internship mentor Dr. Robert Lawrence, who worked closely with me to make sure that I was learning new molecular techniques and understood all the material that was coming my way. I would like to thank Katy Hesser, Matthew McFadden, and the students of the Dr. Ian Hogue lab for their friendship and constant reassurance in my work.

I would like to wrap up by thanking the people in my personal life, my mom and dad, whose sacrifices and love have provided me with the tools I need to be successful in life. Lastly, my fiancé, Jeremy who has spent the last two years encouraging me and supporting my life goals. Thank you, mom, dad, Jeremy for listening to me, allowing me to vent, and giving me the courage to continue. I have had a great support system.

TABLE OF CONTENTS

Page

LIST OF TABLES

LIST OF FIGURES

Figure Page

CHAPTER 1

INTRODUCTION

i. Viral Conformational Changes

All viruses require a host cell in order to carry out replication. The interactions of viruses with their host cells continue to be studied extensively. Techniques used to study these different interactions include virus growth studies and replication basic studies, flow cytometry, confocal microscopy and electron microscopy imaging of infected host cells, and usage of proteomic approaches to analyze a variety of cell cycle proteins that may be affected by virus infection (Emmett et al.).

Viruses are not static structures. There are many steps in the virus lifecycle in which the virus undergoes conformational changes. For example, a crucial step in the lifecycle of all viruses is the translocation of their genome into a host cell. These conformational changes have been detailed for tailed bacteriophages such as bacteriophage T7, that undergo extensive structural remodeling during infection (Hu et al.). However, there are fewer studies that detail the genome delivery of internal membrane containing viruses which include *Corticoviridae, Tectiviridae, Leviviridae* and *Microviridae* families. In a broad sense, understanding changes that viruses undergo during infection can provide insight for development of preventative and therapeutic treatments.

ii. Single Particle Initiative

The study described in this thesis evolved as part of the Single Particle Imaging Initiative (SPI) at the SLAC National Accelerator Laboratory Linac Coherent Light

Source (LCLS). SPI is a large international collaborative effort that focuses on identifying and solving experimental challenges with obtaining high-resolution imaging of single particles using X-ray free electron lasers (XFEL) (Aquila et al.). Members of the SPI team consist of scientists from a variety of fields such as microbiology, biochemistry, biophysics, fluid dynamics, mechanical engineering, optical physics, and computer programming.

The SPI collaboration began with experiments that focused on two model viruses, a plant virus Rice Dwarf Virus (RDV), and bacteriophage PR772. Experiments during multiple beamtimes screened various technical parameters related to sample preparation, sample delivery, X-ray beam characteristics, beam detectors, and data analysis tools. Single particle imaging involves collecting 2D snapshots of individual particles in order to recover a 3D structure, which is accomplished by analyzing a collection of the 2D diffraction snapshots. Diffraction snapshots are obtained from the interaction of single particles with brief femtosecond X-ray pulses that can "outrun radiation damage". The SPI work thus far has laid down the foundation to continue developing XFEL technology to help solve structures for single particle biological samples.

PR772, the focus of this thesis, is a member of the *Tectiviridae* virus family. This family of viruses have an icosahedral capsid that harbors a unique internal lipid bilayer membrane that surround the dsDNA genome (Fig. 1). The internal lipid bilayer is used to translocate the viral genome into a host cell, a property that sets them apart from tailed dsDNA bacteriophages.

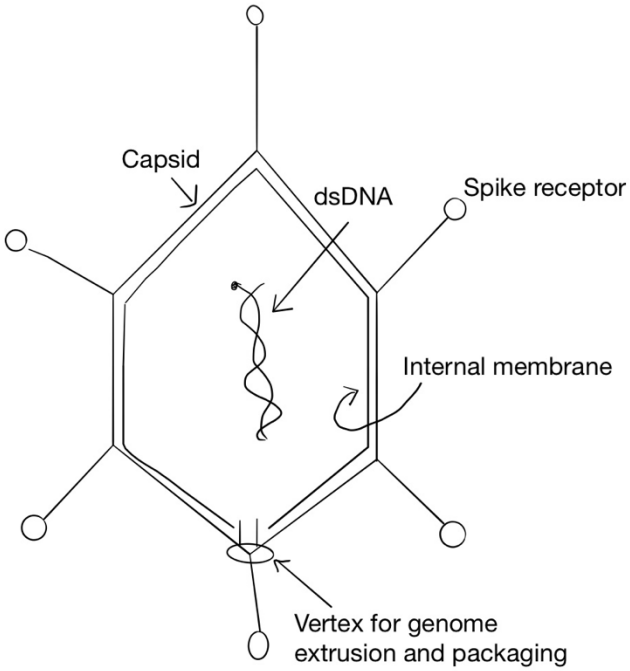

Figure 1. Tectiviridae Structural Characteristics and Features.

Previous research suggests that PR772 and *Tectiviridae* member PRD1 are closely related (Lute et al.). They are both made up of similar proteins, have similar size genome lengths and have a high sequence identity of 97.2%. Both infect gram negative bacteria and share the feature of being icosahedral in shape without tails. At the time that SPI experiments were initiated on PR772 a structure had not yet been determined. However, the structure of PRD1 had been solved using X-ray crystallography and electron microscopy (Abrescia et al.). It was observed that the virion has an exterior icosahedral capsid consisting of protein coat (P3) with receptor-binding spikes (P2) at its vertices and an internal lipidic membrane (Cockburn et al.).

Data collected at LCLS on PR772 yielded a low resolution three-dimensional structure and conformational landscape changes (Aquila et al.; Hosseinizadeh et al.;

Reddy et al.). Data collected from XFEL snapshots were examined without imposing icosahedral symmetry and tubular protrusions were observed in some of the snapshots (Reddy et al.; Aquila et al.; Hosseinizadeh et al.). Given the close relatedness and similarity between PRD1 and PR772, it was concluded that PR772 also uses its internal membrane to form a nanotube-like structure to facilitate genome delivery into the host.

In order to gain insight and understand the virus lifecycle of PR772 the virus structure must be determined. Utilization of developing technology, XFEL and complementary cryoEM in obtaining the structure of PR772 single particles can provide insight into virus-host interaction, genome translocation and viral reproduction.

iii. Objectives/goals

During the initial SPI experiments that produced a low-resolution 9nm 3D structure of PR772, there was a strong focus on the optimization of sample preparation, experimental conditions and data analysis. The work described in this thesis evolved from the initial experiments, with the goal to further optimize PR772 sample preparation to yield cleaner, more homogeneous, high concentration samples for SPI continuing experiments aimed at obtaining a higher resolution 3D structure than was achieved in the initial experiments at the LCLS. In addition to optimizing PR772 samples as part of the SPI team, I also aimed to obtain a high-resolution cryo-EM structure in parallel and to verify if it forms a lipidic nanotube to extrude its genomic content like its relative PRD1. Hong et al., reported that an “aging process”, meaning incubation at 4° C for a period of time, triggers structural remodeling, thus allowing for the observation of the nanotube (Hong et al.). This aging process was conducted on PRD1, and I will be conducting this

aging process on PR772 in order to see if “aging” will allow for observation of the protruding lipidic nanotube.

CHAPTER 2

LITERATURE REVIEW

i. Virus Life Cycle

a. DNA Structure:

There are two types of nucleic acids, deoxyribonucleic acid (DNA) and ribonucleic acid (RNA) (Alberts B). DNA is a double-stranded antiparallel helical molecule. It is composed of four types of nucleotide subunits, which contain a sugar, a nitrogenous base, and a phosphate group (Fig. 2) (Alberts B).

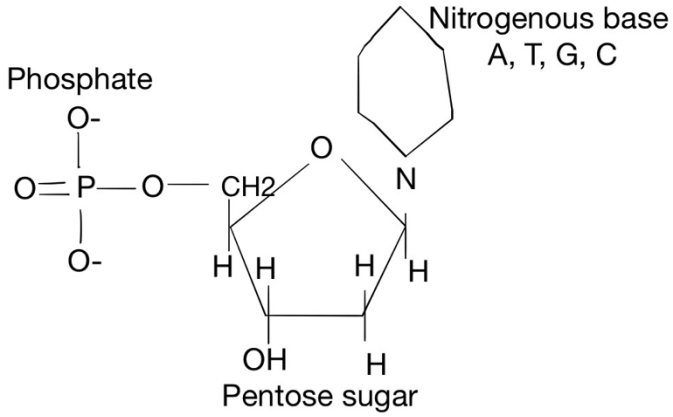

Figure 2. Nucleotide Composition Schematic.

The sugar for DNA is deoxyribose, and the nitrogenous base can be either purines adenine (A), and guanine (G), or pyrimidines cytosine (C) and thymine (T) (Alberts B). These individual bases pair with each other such that A pairs with T and G pairs with C (Chaudhry). Hydrogen bonds between the base pairs bring the two strands of DNA together. The nucleotides are covalently linked together by alternating sugars and phosphates, forming a strand (Alberts B). The sugar of the nucleotides contains a 5' phosphate and 3' hydroxyl group.

b. Viral Genomes

There are 7 types of viral genomes which include double-stranded DNA, + sense single-stranded DNA, double-stranded RNA, + single-stranded RNA, − single-stranded RNA, single-stranded RNA with DNA intermediate, double-stranded DNA with RNA intermediate (Flint et al.). Replication of these different genomes occurs similarly with certain changes in accessories and intermediate steps. For example, all RNA genomes must encode their own RNA dependent polymerase (RdRp) in order to synthesize RNA, or a reverse transcriptase to synthesize DNA from RNA (Flint et al.). Regardless of genome type, all viruses must synthesize mRNA which is decoded using the host translational machinery. The steps to mRNA synthesis vary between different genome types. Single stranded DNA must first synthesize its complement before it can be translated to mRNA, while dsDNA can be transcribed to mRNA. Double stranded RNA contains both + and – sense RNA strand, which can't be translated to synthesize viral proteins; instead, the – strand is first copied into mRNA by RdRp. The synthesized mRNA is encapsidated and copied to make more dsRNA (Flint et al.). + strand RNA can be directly translated into proteins. Replication for + strand RNA is accomplished in two steps. First the complement to the + strand is synthesized and then newly synthesized – strand is copied into full length + strand. Genomes containing + strand RNA with DNA intermediates utilize reverse transcriptase to produce dsDNA that can used to synthesize mRNA and produce more viral genome RNA (Flint et al.). Viruses that contain – strand RNA genomes utilize RdRp to synthesize its complementary + strand mRNA and full length + strands which are used to produce – strand genomes (Flint et al.).

c. Viral Replication

DNA replication is essential for a variety of processes within the cell. Replication begins at the origin of replication, which is composed of sequences that are high in AT content (Chaudhry). These base pairs have fewer hydrogen bonds, making the DNA strands easier to break apart. The basic flow of DNA replication for linear DNA can be seen in Figure 3.

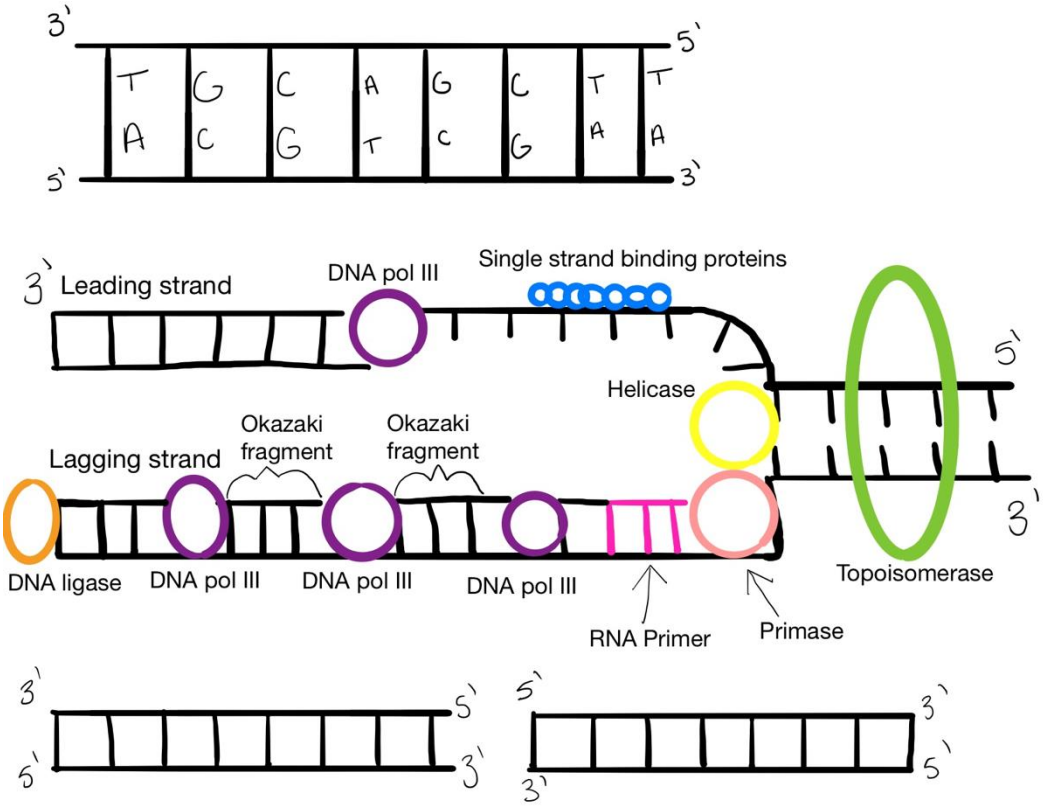

Figure 3. Schematic of Linear Genome Replication.

Topoisomerases I and II aid in reducing pressure on the wound portions of the DNA molecule. DNA replication starts when the enzyme helicase splits apart the two strands of DNA. Single-stranded binding proteins keep the unwound strands separated. The point

along the DNA molecule where helicase is actively splitting the DNA strands is called the replication fork. These two unwound strands are called the leading and laggings strands. RNA primase produces RNA primers that attaches to these strands providing a DNA synthesis starter (Langston and O'Donnell). This RNA primer is where DNA polymerase III attaches to the DNA molecule and begins to attach complementary nucleotides to each now separate strand of DNA. DNA polymerase III traverses a strand of DNA in the 5' to 3' direction, creating the complementary stand (Langston and O'Donnell). For one of the strands, DNA polymerase III travels towards the replication fork. This strand is called the leading strand. For the other strand, DNA polymerase III must travel away from the replication fork. This strand is called the lagging strand. DNA polymerase III cannot traverse the lagging strand continuously. Eventually the DNA polymerase III acting on the lagging strand will either reach the end of the DNA molecule or a region of base pairs already attached by DNA polymerase III. When the DNA polymerase hits either of those sections of the DNA molecule, it will detach and later reattach itself to another RNA primer closer to the replication fork, creating Okazaki fragments. DNA polymerase I replaces the RNA primers with DNA and the fragments are joined by DNA ligase. After the process of DNA replication is complete, each strand from the source DNA molecule will reside in different molecules of DNA (Langston and O'Donnell).

Prokaryotic circular genomes replicate slightly different than eukaryotic DNA replication. Replication of circular genome begins at a specific sequence referred to as oriC (del Solar et al.). There is a single origin of replication unlike the eukaryotic

genome. Within this origin there is a specific sequence that binds with a protein called DNA-A (del Solar et al.). This binding destabilizes the DNA structure, creating a single-stranded opening that is AT rich. This opening is called the replication bubble and it is equipped with two replication forks on each side of the bubble. Single-stranded binding proteins attach to the DNA in order to prevent reannealing of the DNA strands. Helicase pulls apart the DNA strands, which causes positive supercoiling. In order to counteract this, DNA gyrase is attached to introduce negative supercoils, which relaxes the supercoiling and allows DNA replication to continue. DNA primase creates a primer for DNA synthesis. DNA polymerase III then attaches to the DNA using the primer as a starting point. DNA polymerase III attaches new nucleotides to the 3'end of the DNA strands. The top strand, called the leading strand, is able to be continuously synthesized in the 5' to 3' direction while the bottom strand, called the lagging strand, cannot just as in eukaryotic replication. When DNA polymerase III reaches the end of the DNA molecule, it will detach and later reattach itself closer to the replication fork, creating Okazaki fragments. Enzyme RNase H catalyzes cleavage of RNA where DNA polymerase I attaches and synthesizes new nucleotides. The fragments are then joined together by DNA ligase.

As for plasmid DNA, it uses a mechanism called the rolling circle replication system (Rampersad and Tennant). Similar to both eukaryotic and circular bacterial genomes, replication is started by an initiator. For plasmids the initiator is protein RepA which binds to the origin of replication and cuts one strand of the DNA. RepA holds on to the 5' end of the cut DNA strand while the 3' end with an exposed hydroxyl group acts

as a primer for DNA polymerase III (del Solar et al.). DNA polymerase III then replicates the intact complementary DNA strand. Helicase is recruited by RepA to unwind the DNA from the 5' side where single strand binding proteins attach to prevent reannealing of the DNA strands. The unwinding of the 5' strand continues to occur until replication of the intact complementary strand is complete. The two ends of the cut strand are put together by RepA and released, forming a circular strand, while the replicated complimentary strand is sealed by DNA ligase. The circular single stranded DNA is then replicated. The strand forms a loop where RNA polymerase attaches and acts as a primer. DNA polymerase III uses the primers to begin synthesizing the new strand of DNA. Ligase seals the remaining cut, forming a double stranded plasmid.

There are two known mechanisms for the synthesis of double-stranded viral genomes. These methods proceed by either copying both strands at a replication fork or coping only one strand while its complement is removed, which is known as strand displacement (Flint et al.). These types of replication mechanisms have been previously described. Viral RNA genomes never use the replication fork mechanism. DNA synthesis using the replication fork mechanism needs an RNA primer and has the formation of Okazaki fragments. The strand displacement mechanism requires a primer, but it is not an RNA primer. Instead the primer is dependent on the virus. Examples of primers for strand displacement include DNA hairpins and proteins. The primer for adenoviruses is a protein primer, called precursor terminal protein pTP (de Jong, Meijer and van der Vliet). Viruses with linear DNA genomes use this stand displacement mechanism for DNA synthesis while viruses with circular DNA genomes, such as herpesviruses and lambda

phage, use the replication fork mechanism. The rolling circle replication system has been highlighted for dsDNA viruses such as herpesviruses. Herpesvirus replication has multiple cycles of copying the circular template. This is proceeded by discontinuous DNA synthesis on the cut single strand. This produces linear dsDNA molecules that contain concatemers, meaning multiple copies of the genome (Rampersad and Tennant).

d. Assembly and Genome Packaging

There are two possible assembly pathways for viruses, concomitant assembly or sequential assembly (Ahi and Mittal). The capsids in concomitant assembly are assembled around the viral genome. This is commonly seen in helical viruses, spherical retroviruses, and some icosahedral viruses. A majority of icosahedral viruses use the sequential assembly mechanism where the empty capsid or procapsid is initially assembled before the viral genome is packaged. Viruses with different genomes and synthesis mechanisms require different or additional enzymes and packing related proteins. For example, viruses with concatemeric genomes such as herpes simplex virus need terminases that translocate and cut DNA (Sun, Rao and Rossmann; Newcomb et al.). Terminases are made up of small and large subunits. The small subunit oversees recognition, binding of viral DNA, and activation of ATP hydrolysis, while the large terminase subunit carries out cleavage activities (Sun, Rao and Rossmann; Karhu et al.). Cleavage for packaging of concatemeric DNA can be done at an independent sequence via a head full packaging mechanism or a specific sequence. For lambda phage it is done at a specific site called cos sites, while phages SPP1 and P22 use the full head packaging mechanism (Coren, Pierce and Sternberg). With the full head packaging system, the size

of the genome to be packaged is dictated by the size of the viral capsid that will surround the genome (Coren, Pierce and Sternberg). After completion of packaging and cleavage, the packaging terminase DNA complex dissociates and binds to another procapsid for genome packaging (Karhu et al.). For viruses such as bacteriophage phi29, which is equipped with unit length genomes, cleavage is not necessary. Viruses with unit length genomes utilize ATPase for genome packaging. Similarly, to adenovirus and PRD1, phi29 uses a protein primer for its genome replication. Additionally, more packaging-related proteins have been identified and it has been hypothesized that these proteins are actually a part of the packaging machinery. An example of these types of proteins include, but are not limited to, stabilization and sealing proteins. Sealing proteins ensure that the packaged capsids will not release their packaged DNA. Herpes simplex virus type 1 proteins UL17 and UL25 stabilize mature virions by binding on the capsid, outside the packaging machinery (Karhu et al.). Occasionally host proteins have been observed to play a part in the packaging process, such include bacteriophage lambda whose integration host factor is thought to govern its' packaging machinery (Karhu et al.).

An important process in the virus life cycle is genome packaging. Many viruses package newly synthesized DNA into pre-formed procapsids. This process involves a variety of viral proteins and a packaging motor protein that utilizes ATP molecules as energy currency that is converted into mechanical energy by ATP hydrolysis (Sun, Rao and Rossmann). The hydrolysis of ATP aids in the condensation of the genome. The genome is then transported into the procapsids by packaging ATPase or terminase through a portal vertex. The portal vertex is the location where packaging proteins

anchor. The portal vertex is equipped with portal proteins that are part of procapsids and mature capsids, unlike terminase proteins which are exclusively in procapsids (Newcomb et al.).

Several components of the genome packaging process differ among a variety of viruses. For example, viruses equipped with a dsRNA genome keep their packaging motor after termination of packaging as a component of the final viral particle while the dsDNA genome packaging motor detaches once packaging is complete (Sun, Rao and Rossmann). The packaging motor of dsDNA viruses typically have two domains. These domains consist of a N-terminal ATPase domain and a C-terminal domain with nuclease activity (Sun, Rao and Rossmann). Furthermore, there are viruses that use terminase for genome packaging. Terminase is made up of a large and small subunit that are involved in the packaging process. Viruses whose genomes are replicated as concatemers use these terminase subunits for genome packaging. The small terminase subunit works with the large terminase subunit for packaging initiation and further refines the large terminase activity during packaging (Sun, Rao and Rossmann; Catalano). Terminase aids in packaging by preparing the genome through a site-specific endonuclease reaction which results in the recruitment of a procapsid triggering the insertion of the genome through an ATP-dependent manner. The packaging process is completed when terminase cuts the end of the viral genome (Catalano).

Phage λ produces concatemeric DNA that is cut by terminase at specific sites, packaged and translocated into the prohead, a procapsid precursor (Catalano, Cue and Feiss). Similarly, herpes simplex virus type 1 (HSV-1) has a concatemer genome that is

synthesized and packaged in the host nucleus. Pre-formed capsids are assembled in the nucleus where the concatemeric DNA is cut by terminase and packaged into capsids. The terminase attaches to the portal of the progeny procapsid and inserts the genome via energy produced from terminase catalyzed ATP hydrolysis (Newcomb et al.; Poon and Roizman). The process is complete once terminase makes a second cut in the DNA, ultimately sealing the portal. HSV-1 closely resembles the genome encapsidation process of dsDNA bacteriophages, such as λ phage. Bacteriophages, including λ phage, begin assembly with the formation of empty procapsids that have a unique portal vertex for genome insertion and release. HSV-1 encodes a homolog of phage T4 terminase, protein UL15, that was confirmed by amino acid sequencing. Furthermore, HSV-1's portal has similarities to the portals of dsDNA bacteriophages, such as the inner and outer diameters of their packaging portal (Newcomb et al.). Several studies have highlighted the roles of several packaging proteins encoded by HSV-1. A study done by Poon et al. showed that mutations in the open reading frames of the UL15 gene did not allow for packaging of the genomic DNA (Poon and Roizman). Additionally, UL6, UL15, UL17, UL25, UL28, UL32, and UL33 have been shown to also be involved in DNA packaging (Newcomb et al.). Confirmation of the roles of these genes in DNA packaging was done by generating mutants that lacked UL6, UL15, UL17, UL25, UL28, UL32, and UL15 function. Cells were infected with these mutants and the result was DNA replication and capsid formation but packaging inhibition(Newcomb et al.).

Similarly to HSV-1 and λ phage, the PRD1 genome is packaged through a vertex into preformed capsids using virion associated packaging protein ATPase P9 (Ahi and

Mittal; Cepko and Sharp). Unlike HSV-1 and λ phage, PRD1 does not synthesize concatemeric dsDNA and does not use a terminase to aid in packaging of its genome. Instead, PRD1 is hypothesized to resemble Adenovirus's (AdVs) genome packaging mechanism due to the similarities between the two viruses. Adenoviruses, belonging to the Adenoviridae family are icosahedral non-enveloped viruses equipped with a linear dsDNA genome. Structural and architectural features were compared between adenovirus and PRD1. This led to the revelation that adenovirus's and PRD1 have a number of similarities leading to the belief that these two viruses originate from a common ancestor (Strömsten, Bamford and Bamford; Karhu et al.). These similarities include a major coat protein fold, a T=25 capsid arrangement which is not observed in other viruses, a common vertex organization, a linear genome with inverted terminal repeats, and 5' terminal proteins which allow for protein-primed DNA replication (Strömsten, Bamford and Bamford). Lastly, they are both equipped with receptor-binding spikes at their capsid vertices (Karhu et al.; Ahi and Mittal). Both these viruses follow a sequential assembly mechanism where empty procapsids are assembled and the unique vertex on the capsid equipped with an ATPase aids in the packaging of its genome (Ahi and Mittal). Although they do share a variety of similarities, they differ in that AdV lacks a membrane

e. Envelope Classification

Viruses are classified as being enveloped or non-enveloped viruses. Enveloped viruses possess their membranes as an outer envelope or as an internal membrane enclosed within a capsid. The entry of both these types of viruses require the interactions between host cell receptors and viral-encoded envelope or capsid proteins. Outer

enveloped viruses fuse their membranes with the plasma membrane or endosomal membrane of their host, allowing for the release of its capsid into the host cytosol. Membrane-containing bacteriophages gain entry and release of their genome through a slightly altered mechanism. Membrane-containing bacteriophages have provided an ideal model for studying membrane biosynthesis, structure, and function (Mäntynen et al.). Membrane-containing bacteriophages can be subdivided into three subclasses based on the location of their membrane. These subclasses include viruses whose membranes are within a capsid, viruses whose membrane encompasses the virus capsid, and lastly viruses who lack a rigid protein capsid and are equipped with a pleomorphic proteinaceous lipid vesicle which encompasses its genome (Mäntynen et al.). These subclasses also have their own mechanism for making contact and gaining entry into their host. These mechanisms are similar to those used by enveloped viruses. The entry mechanism for phages having an outer lipid membrane involves the attachment to a pilus that retracts, thus bringing the virus into contact with the host's outer membrane. The viral membrane fuses with the host membrane, leading to the release of the nucleocapsid into the hosts periplasmic space (Mäntynen et al.). This space is located between the membranes of the host bacteria. To gain access to the cytoplasm, virus-encoded lytic enzymes digest the host peptidoglycan layer where the nucleocapsid enters through an endocytic route. The nucleocapsid dissociates, releasing the viral genomic content (Mäntynen et al.). Unlike enveloped viruses, the internal containing membrane phages have their membrane within the virus capsid. Internal membrane phages make contact with their host through host receptor interactions. This interaction triggers the formation

of a proteolipid tube that passes through the host envelope, providing a conduit for genome delivery into the cytoplasm (Mäntynen et al.). Lastly there is another mechanism that pleomorphic phages use for making contact and delivering their genome to their host. This mechanism includes the use of host receptors. The phage binds to the host receptor causing the dissociation of the viral protein capsid, triggering the fusion of the viral internal membrane and the outer membrane of the bacterial host. Therefore, the viral genome is inserted into the host cell (Mäntynen et al.). Bacteriophages such as PRD1 do not fuse their internal membrane with the host outer membrane. Instead this phage undergoes conformational changes, triggering the production of a lipid tube that passes through the host outer membrane acting as conduit for genome release (Mäntynen et al.).

f. Envelope Sequestering

Newly synthesized virions obtain their lipid membranes through a variety of mechanisms. For many enveloped viruses, the process of obtaining their external membrane is done during budding. The nucleocapsid can bud through the host cytoplasmic membrane or intracellular membrane structures. These intracellular membrane structures include the endoplasmic reticulum, intermediate compartment, Golgi or *trans*-Golgi network (Thorley, McKeating and Rappoport). Unlike enveloped viruses, bacteriophages have not been shown to use budding as a mechanism for egress and lipid membrane sequestering (Thorley, McKeating and Rappoport). Assembly of PRD1 is initiated by the recruitment of synthesized capsid proteins and phage-encoded membrane proteins. A phage specific membrane patch is pinched off the host cytoplasmic membrane using a process that resembles clathrin-mediated endocytosis of

eukaryotic cells, which results in the formation of a vesicle that is hypothesized to act as a scaffold for capsid protein assembly (Mäntynen et al.) This membrane patch contains nonstructural protein P10 that is displaced to form an empty procapsid. The genome is then packaged within these preformed procapsids through a unique vertex using packaging ATPase P9. This is similar to tailed bacteriophages which also package their genome within preformed procapsids (Strömsten, Bamford and Bamford). The mature virions are then released by host cell lysis, which uses a holin–endolysin system to degrade the cytoplasmic membrane and peptidoglycan layer (Mäntynen et al.; Strömsten, Bamford and Bamford). This system uses holin proteins which are phage-induced integral membrane proteins that gives lytic enzymes access to the host cell cytoplasmic membrane and peptidoglycan layer (Strömsten, Bamford and Bamford; Rydman and Bamford; Mäntynen et al.).

g. Envelope Function

Viruses have evolved to use their membranes in a variety of processes throughout their lifecycle. It is important to note that these viruses gain their envelopes from the host cell during assembly and egress. Viral proteins, often glycoproteins, are anchored in the viral envelope. These viral membranes are diverse in size, morphology, complexity and vary in lipid composition, protein content, and location. Envelopes form the outer regions of animal viruses, but archaeal viruses as well as bacteriophages have their membranes located beneath an icosahedral capsid (Flint et al.).

Within the membrane are viral proteins such as integral membrane proteins that are held in the lipid bilayer by a membrane spanning domain (Flint et al.). These integral

membrane proteins, also known as envelope glycoproteins, carry oligosaccharides. These sugars are usually added to the proteins during transport to the cell membrane (Flint et al.). The membrane spanning domain separates the large external domain and small internal segments. These segments are important during different stages of the virus lifecycle. For instance, the large external domain has binding sites for cell surface virus receptors, major antigenic determinants, and fusion mediators, while the small internal segment is important for virus assembly (Flint et al.). Furthermore, the viral membrane glycoproteins form oligomers that are bound by non-covalent interactions and disulfide bonds (Flint et al.). These oligomers can form spikes, that are used for contact with host receptors. Coronaviruses assemble and bud intracellularly and are an example of a virus that derives its membrane from a different host cellular membrane, the ER-Golgi intermediate compartment (ERGIC) (Flint et al.; Ruch and Machamer). There are three modes of interaction of capsids or nucleocapsids with envelopes of virus particles, direct contact, contact via a matrix protein, and contact via a multiprotein layer. In the case of coronaviruses the nucleocapsid interacts with the carboxy tail of the membrane (M) protein to drive the budding process at ERGIC membranes (Hogue and Machamer)

Envelopes, whether internal or external, aid viruses in entry of either the genome or whole virus particle. Not all enveloped viruses fuse at the cell surface, many are endocytosed and then fuse with the endosome membrane. While the membranes are in different locations and used differently, the goal for each is to successfully initiate the infection by releasing the core of virus or its' genome into the host cell. The location of these envelopes may be linked with the virus's ability to survive the environment they are

in. For instance, envelopes are sensitive to environmental changes, such as lipid solvents, pH, and temperature. Impairment of the envelope may cause the virus to lose infectivity. Many of these outer enveloped viruses have evolved to evade the host immune system by attaining their envelope from the host, making them less prone to be identified as foreign by immune cells (Flint et al.). Bacteriophages such as PRD1, which have been extracted from sewers, may have an internal membrane to survive the extreme conditions in which they are found. They ultimately "hide" their membrane within their capsid in order to preserve their genome conduit.

ii. *Tectiviridae* Family:

Tectiviridae is a family of viruses that is made up of a sole genus (Jalasvuori and Koskinen). This genus is the Tectivirus which consists of tailless bacteriophages. Common features of this family are the presence of an internal membranes that contains a ~15kb linear dsDNA genome. The internal lipid membrane is a unique characteristic that is commonly used to translocate the viral genome, a characteristic that sets them apart from tailed dsDNA bacteriophages (Jalasvuori and Koskinen). This virus family has an internal membrane and lacks an external envelope; instead its icosahedral capsid that is about 70nm in diameter has flexible spikes that extend from the virion vertices (Jalasvuori and Koskinen; "Family - Tectiviridae"). The genomes contain 30 genes and are equipped with inverted terminal repeats and terminal proteins that are covalently linked at the 5' end. The covalently-linked proteins are used as replication primers, and the genome is replicated using phage-encoded polymerase (Jalasvuori and Koskinen). DNA entry, replication and transcription are followed by the polymerization of capsid

proteins. A membrane containing procapsid is formed by nonstructural virion-encoded assembly factors, coat-forming proteins, and a virus-specific lipoprotein membrane (“Family Tectiviridae”). The procapsid is transported inside the cell where the genome is packaged through a unique packaging vertex using portal proteins and an enzyme called terminase or packaging ATPase ("Family - Tectiviridae"). A variety of virus portal protein structures have been solved and they all have a cone-like shape. This internal membrane is made up of viral proteins and lipids from the host plasma membrane. The viruses in this family infect both gram-positive and gram-negative bacteria. Genome sequence comparison confirmed that this family is highly similar but were subdivided by their choice of host. The viruses that infect gram-negative bacteria are PR5, PR3, PR4, L17, PRD1, and PR772 (Saren et al.). Viruses Bam35, GIL01 and GIL16 infect gram-positive bacteria.

Model *Tectiviridae* family phage PRD1 is a lytic enterophage with a linear dsDNA genome whose replication is protein primed and proceeds by strand displacement. Replication occurs on both ends of the genome since the inverted repeats have an origin of replication. The capsid has spikes, consisting of viral proteins P2 and P5 which extend from P31 a penton protein at the virion vertices, and are used for receptor recognition (Gowen et al.). The capsid also contains a packaging vertex for PRD1 which uses ATPase P9 and three other proteins for packaging newly synthesized DNA within the inner membrane. Mature PRD1 virions are released by lysis of the host cell.

iii. PRD1 & PR772: Previous Studies

Genome packaging and delivery are an important step in the viral life cycle. The genome delivery and entry of tailed dsDNA bacteriophages has been well studied although little is known about viruses that contain an internal membrane vesicle. dsDNA bacteriophage genomes are typically wound around an axis as the DNA rungs through a packaging vertex during assembly (Cockburn et al.). Tailed dsDNA phages characteristically have genome injecting machineries as part of the particle structure that is formed during assembly. The genomic DNA exits through the tail when the viruses infect with the bacterial host (Santos-Pérez et al.). Tailed viruses of different families, such as the *Myoviridae* family, store energy in their tails used for tail tube penetration, while viruses with non-contractile tails, such as the *Podoviridae* family and the *Siphoviridae* family, are not known to rely on stored energy for infection (Leiman et al.; Molineux and Panja).

Bacteriophage PRD1 is a tailless icosahedral virus with an internal membrane that surrounds the genome. Contact with its host causes PRD1 to undergo remodeling and extrusion of a proteolipid tube that is used for ejection of the genome during infection (Grahn et al.; Abrescia et al.; Karhu et al.; Cockburn et al.). PRD1 was confirmed to contain an internal lipid membrane by cryo-EM tomography and electron density mapping (Cockburn et al.). Distances from the particle center along the icosahedral 3-fold axis were measured and a fall was observed in the density map which represents the leaflets of the internal membrane (Fig. 4) (Cockburn et al.). The lower panel of Figure 4

shows the space filling representation which is based on the electron density analysis of PRD1 (Cockburn et al.).

This internal membrane plays a role in infection of PRD1, sustaining the force required for DNA ejection and opposing internal turgor pressure from the host (Cockburn et al.; Santos-Pérez et al.). The PRD1 genome is capped with terminal protein P8 and

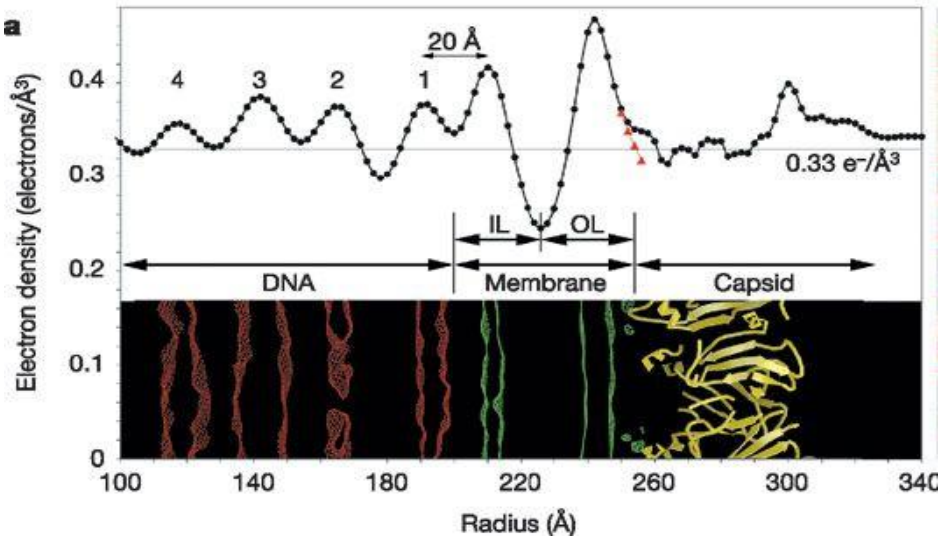

Figure 4. Electron Density Profile of PRD1 with Corresponding Positions of Genomic DNA, Inner and Outer Leaflets of the Internal Membrane [Cockburn et al.].

packaged using a complex made up of ATPase P9, packaging accessory protein P6, and two small membrane proteins P20 and P22 within a preformed membrane containing procapsid (Coetzee and Bekker; Peralta et al.; Schijven, Sadeghi and Hassanizadeh). The additional 11 vertices are made up of vertex-stabilizing membrane protein P16, penton protein P31, spike protein P5, and receptor binding protein P2 (Schijven, Sadeghi and Hassanizadeh; Coetzee and Bekker; Peralta et al.). PRD1 infection is activated by binding of P2 to the host cell receptor.

PR772 is thought to behave similarly to PRD1. PR772 is also a member of the *Tectiviridae* family. PR772 was chosen for X-ray free electron laser (XFEL) SPI experiments in order to determine its 3D structure. Snapshots of PR772 were collected at the AMO end station during a number of LCLS SPI experiments. Snapshots of PR772 were collected during a number of SPI experiments. The data collected during these experiments have been analyzed by several groups (Reddy et al.; Hosseinizadeh et al.). The analysis done by Hosseinizadeh et al., to which the Hogue Lab contributed, is summarized here (Hosseinizadeh et al.). 37,550 snapshots were selected from a dataset consisting of 135,375 total snapshots and information was extracted from these experimental single-particle XFEL snapshots using a geometric machine learning approach based on an algorithm developed by BioXFEL and SPI collaborators. An example of the snapshot diffraction pattern taken during the numerous beam times can be seen in figure 5. The image shows the diffraction pattern produced from the beam coming into contact with a single virus particle.

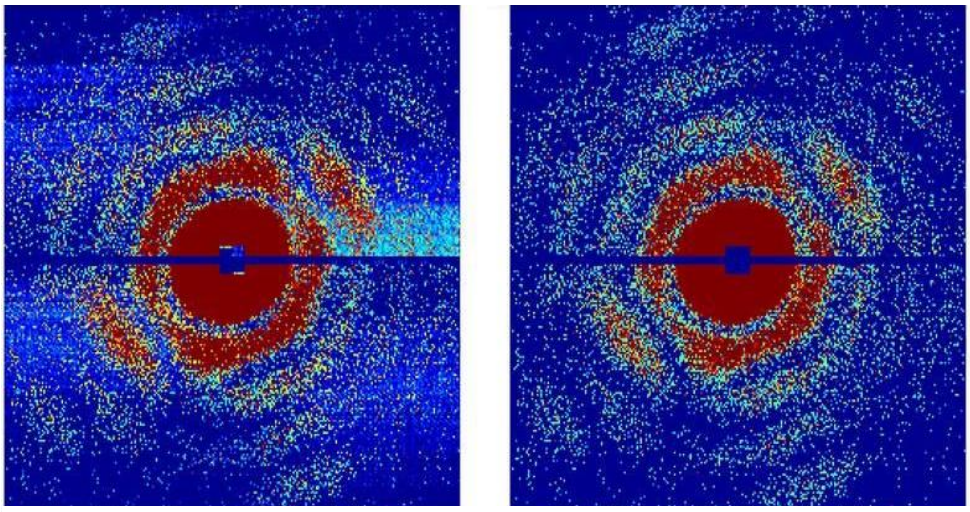

Figure 5. Diffraction Snapshot Example of PR772[Hosseinizadeh et al].

From this a 3D diffraction volume was determined for PR772 with a corresponding 9nm resolution structure (Fig. 6). This averaged structure was based on the assumption that the sample was made up of a homogeneous viral population.

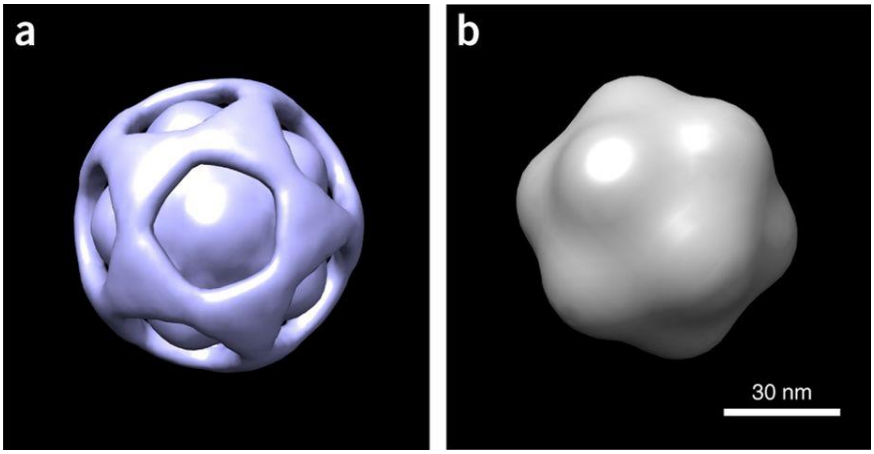

Figure 6. 3-D Diffraction Volume (a) and Corresponding Structure (b) [Hosseinizadeh et al.]

The individual snapshots were examined, and a comparison between snapshots suggest that structural heterogeneity was present. Similar snapshots were sorted into bins and a conformational spectrum was defined based on a single dominate conformation coordinate. Individual conformations were reconstructed and an increase of ~11% in diameter and a corresponding reduction of ~68% decrease in inner density was observed over the full conformational range (Fig. 7). This is reminiscent of what has been described as virus "swelling" (Hosseinizadeh et al.).

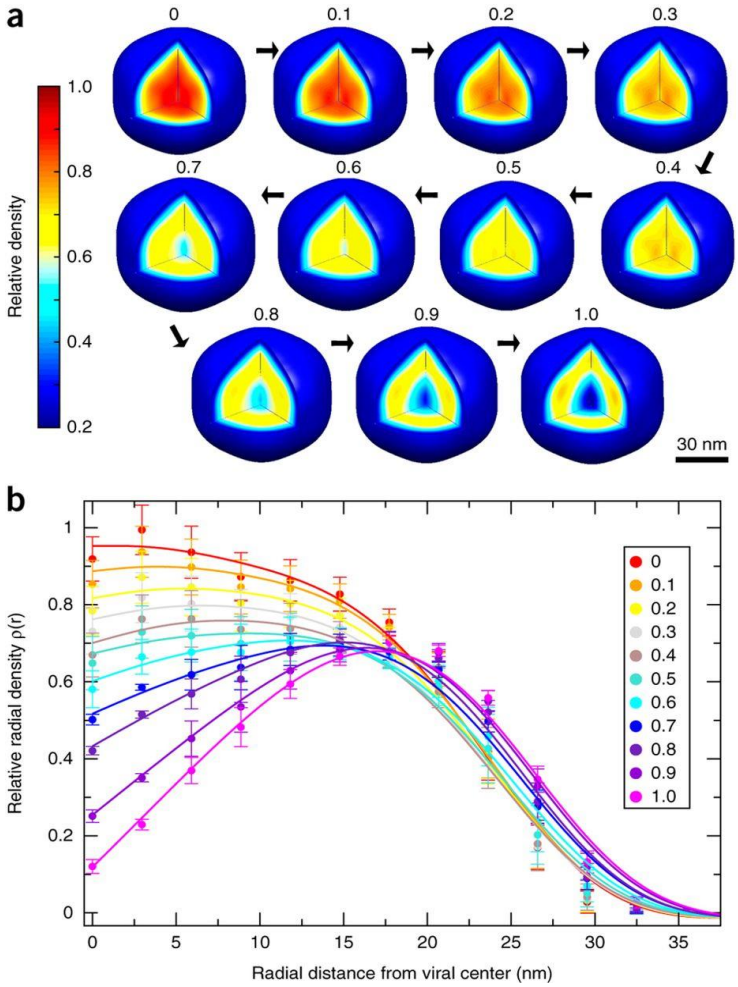

Figure 7. 3D Structures Assuming Icosahedral Symmetry [Hosseinizadeh et al.].

As the team thought about what the conformational range might mean, there was some new results that were published that described PRD1 and the release of a proteolipid nanotube (Fig. 8).

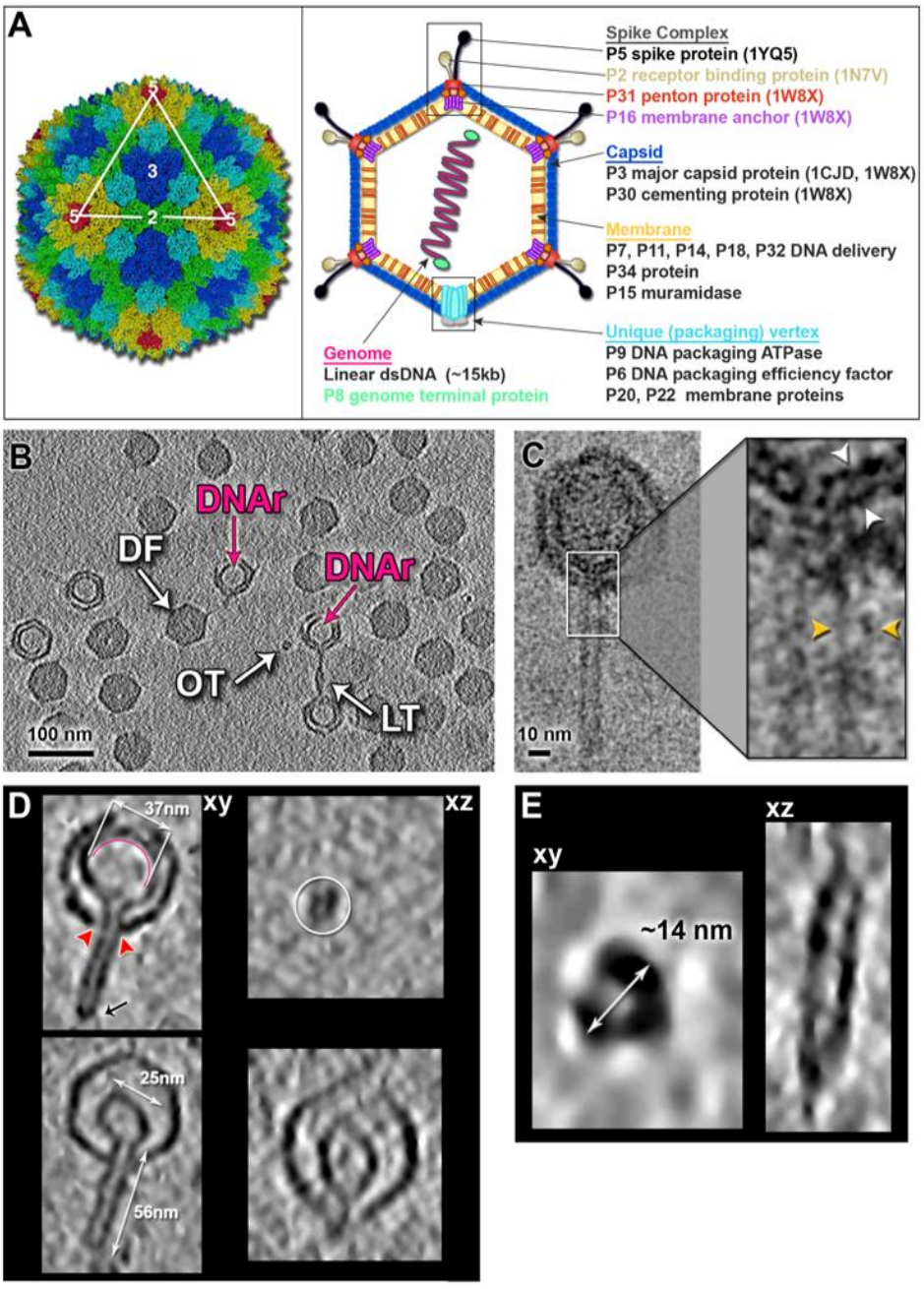

Figure 8. Cryo-ET Structure of PRD1 With A Tail Tube [Peralta et al.].

Perala et al. using cryo-electron tomography (cryo-ET) highlighted the mechanism PRD1 utilizes for genome translocation across the host envelope. Cryo-ET is a technique that utilizes electron microscopy for data collection, tomography for visualization in all angles, and vitrification for sample preparation (Koning). Electron tomography images the sample at different angles by rotating the microscope stage in order to move around the center of the sample (Koning; Peralta et al.). The diffraction snapshots were subsequently reexamined without imposing icosahedral symmetry and a tubular protrusion was observed in some of the individual snapshots obtained by phasing 2D XFEL diffraction patterns (Fig. 9).

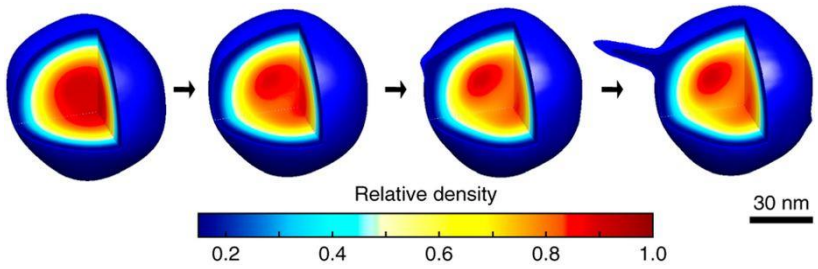

Figure 9. 3D Structures Without Imposing Icosahedral Symmetry [Hosseinizadeh et al.].

This was interpreted to be proteolipid tubes, similar to what was observed for PRD1. These tubes were observed in reconstructions that lacked icosahedral symmetry, but tubes were not observed in the 3D reconstructions which assumed icosahedral symmetry. These results indicate that a single conformational coordinate controls reorganization of the genomic content, growth of a lipidic tubular structure and genome release (Hosseinizadeh

et al.). Thus, PR772 appears to behave similarly to PRD1in that a tubular membrane undergoes conformational changes in order to deliver its genomic content during infection. The host receptor for PR772 which likely helps trigger the nanotube formation has not yet been discovered.

iv. Methodology used for propagating and purifying viruses:

a. Propagation: Soft agar overlay

There are a variety of methods used to propagate and purify viruses. These methods are dependent on the type of virus and host cell. The soft agar overlay method was developed over 70 years ago for use in microbiological research, including work with bacteriophages, and other bacteria that produce bacteriocins and proteinaceous antibacterial agents (Hockett and Baltrus). This method produces a homogenous lawn of bacteria within a thin layer of cooled 0.5% agar. The soft agar/bacteria can be spotted with dilutions of a virus to titer a stock or virus can be added to the mixture of 0.5% agar and bacteria leading to infection and virus production. This method requires minimal resources and is inexpensive. Liquid cultures may also be used that are also inexpensive and require minimum resources. PR772 titers are higher when grown using the overlay method. Additionally, liquid cultures require that both phage and bacteria become diluted prior to initiating infection in order to assure that the bacteria does not outgrow the virus.

b. Fast Protein Liquid Chromatography (FPLC) and Ultracentrifugation

Purified samples of proteins and viruses are necessary for different types of experiments, including structural studies and biochemical assays. These studies require highly purified, concentrated, homogenous samples. Several factors must be taken into

account when choosing a purification method including, the least amount of manipulation and number of steps. This helps ensure a yield that has the highest functional protein and highest quality virus particles. Furthermore, completing these steps at 4°C will help ensure that proteins and virus particles do not undergo proteolysis and that their structural integrity is maintained. There are several purification methods available which include: density gradient ultracentrifugation, pelleting viruses by centrifugation, ultrafiltration, and chromatography (Nasukawa et al.). Adding cushions while ultracentrifugation of a sample can help maintain the structural integrity of the sample. For years ultracentrifugation through a cesium chloride (CsCl) density gradient has been utilized. The CsCl gradient separates particles based on their buoyant density, yielding a highly homogenous virus sample. Figure 10 shows a schematic of the CsCl gradient that was utilized to purify and concentrate bacteriophage PR772. It shows how this method allows for separation of empty virus particles from whole particles which can be used for further analysis of the virus.

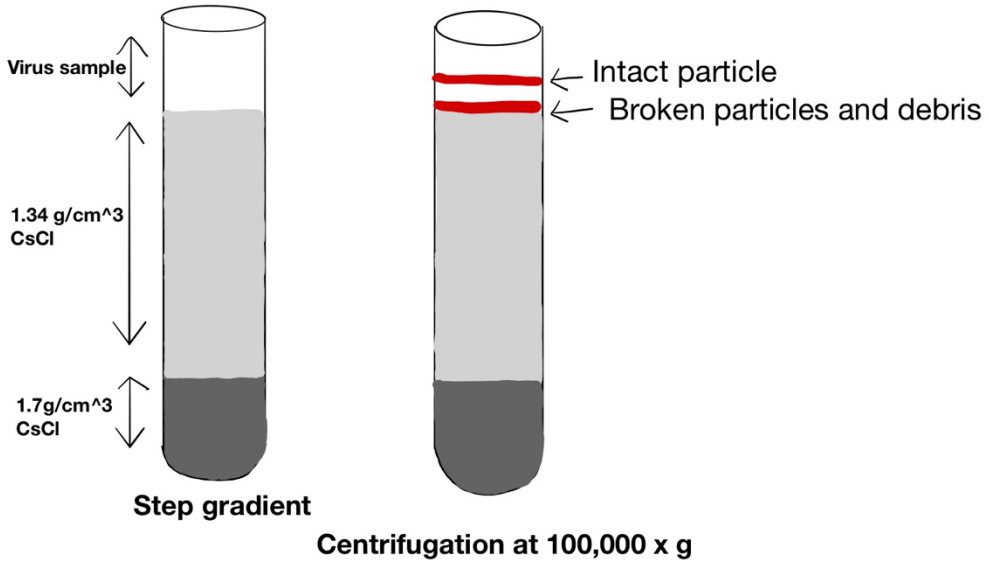

Figure 10. CsCl Step Gradient Purification Schematic.

Some bacteriophages cannot be purified using this method because of their instability in the high osmotic environment of CsCl gradients (Nasukawa et al.).

Fast protein liquid chromatography (FPLC) coupled with ion exchange chromatography (IEX) are used extensively to produce high purity, concentrated viral samples. IEX separates proteins and viruses based on net surface charge and electrostatic interactions that exist between the sample and the column resin (Caroline). There are two types of IEX: anion and cation exchange. Anion exchange columns have positively charge stationary phase resin that binds to negatively charged particles while cation exchange columns have negatively charged stationary phase resin that binds to positively charged particles (Fig. 11). These stationary phases are made up of inert agarose-based or polymeric matrices with a covalently bound charged group (Caroline). Proteins exhibit a net charge that is dependent on the amino acid composition, covalently attached

molecules, and pH of the buffer (Caroline). The isoelectric point (pI) is the point at which the protein is at a pH where it has no net charge. There are online tools that help calculate the theoretical pI of a protein. A pH above the pI yields a protein with a net negative charge while a pH below the pI yields a protein with a net positive charge. This allows for adjustments to facilitate binding to the IEX column and elution. It is important to consider the stability of a protein when choosing purification conditions and column selection.

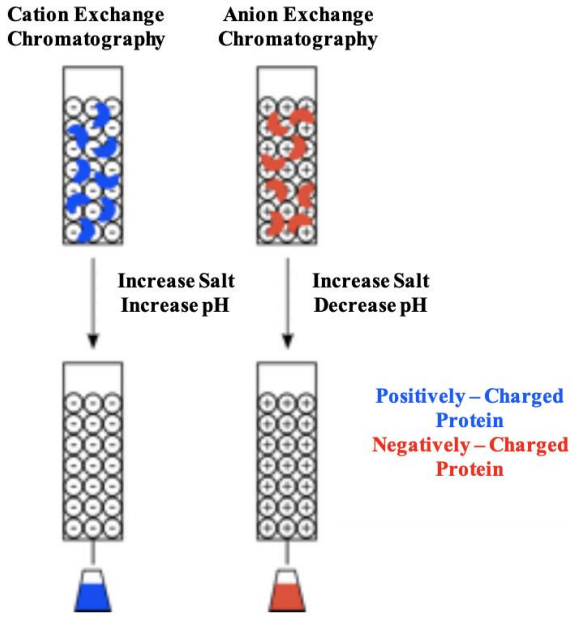

Figure 11. Ion Exchange Chromatography [Caroline]

Anion-exchange chromatography is a technique used to separate impurities and produce concentrated samples. Anion exchange matrices generally have one of two types of charged functional groups: quaternary ammonium (Q), or diethylaminoethyl (DEAE). Charge functional group Q is a strong anion exchanger while DEAE is a weak anion exchanger. Strong exchangers are used when the pH for binding is either acidic or basic since the functional groups remain charged over a range of pHs. Weak exchangers show

weaker retention, enabling elution at lower ionic strength (Caroline). The stationary phase of IEX requires an equilibration step with low ionic strength buffer before being loaded with sample that is also resuspended in a low ionic strength buffer. The sample is bound to the resin and eluted using a step gradient with a buffer of high ionic strength such as NaCl. The addition of salt onto the column introduces ions that compete with the bound proteins for functional groups on the stationary phase (Caroline). As the concentration of NaCl is increased, the number of ions competing to bind to the columns functional groups increases (Caroline). This allows for impurities and lastly the protein of interest to elute from the resin. Purification of phages using anion-exchange chromatography requires optimization which can include buffer composition, binding and elution conditions, and column selection (Caroline).

v. Characterization and Data Collection Methods

a. Enumeration

After purifying a sample, it must be is characterized to determine the quality of the preparation, including purity, concentration or titer, and particle integrity. These types of characteristics can be analyzed using different techniques. Viruses can be visualized by EM to give insight about the purity, concentration and particle integrity. The titer (pfu/ml) of infectious virus can be determined using a plaque assay. Plaque assays are a reliable accurate method used to quantify infectious virions through the counting of plaques (Baer and Kehn-Hall). During a plaque assay, a layer of host cells is infected with a virus of varying concentrations. An immobilizing overlay is added on top of the monolayer to prevent random virus spreading (Baer and Kehn-Hall). Low melting

agarose, methylcellulose and other semisolid media are commonly used as the overlay in plaque assays. Plates are allowed to incubate until plaques form and depending on the overlay applied and characteristics of the plaques, a stain may be used to better visualize the plaques. Plaque morphology can be also used to provide insight about the growth properties of a virus. Plaques are counted, and the titer is calculated using the equation:

$$\frac{Pfu}{mL} = \frac{Average\ \#\ of\ Plaques * Diluion\ Factor\ (Recipricol\ of\ Dilution)}{Volume\ of\ Diluted\ Virus\ Added\ to\ Plate}$$

Although there are a variety of methods that can be employed to quantify virus such as, immunoassays, flow cytometry, and quantitative reverse transcription polymerase chain reaction (qRT-PCR) these methods do not quantify only infectious virions. Not all viruses are lytic and form plauqes, thus different methods are used to quantify non-lytic viruses. Focus forming assays (FFAs) do not count on cell lysis and counterstaining but instead use immunostaining to identify intracellular viral proteins using tagged antibodies (Baer and Kehn-Hall). Although this method allows for tittering of non-lytic viruses it is limited by its inability to probe for infectious virions and requires antibodies. For the purposes of the study, plaque assays using the soft agar overlay were employed.

Protein concentration can be determined using assays such as the Lowry assay and Bradford assays. Sodium dodecyl sulfate polyacrylamide gel electrophoresis (SDS-PAGE) can also be used to estimate protein concentration. SDS-PAGE is a method used to determine size and separate a mixture of proteins using a gel matrix and migration in the presence of an electric current. The rate at which the proteins travel through the gel matrix is dependent on the charge, size, and shape of the protein (Manns).

Nanoparticle tracking analysis (NTA) by NanoSight and Dynamic light scattering (DLS) can give insight into the size and monodispersity of a sample. NTA measures size distribution and concentration in real time by using laser light scattering and Brownian motion (Vestad et al.). NTA determines the Brownian motion by video analysis, where suspended particles are visualized by illumination (Vestad et al.). Laser light is passed through the sample chamber where it comes in contact with particles. The particles are hit by the laser beam and the scattered light is recorded using a light sensitive camera allowing for determination of sample size distribution and concentration (Fig.12). DLS works a little differently, it is dependent on the intensity of the light scattering, which requires knowledge about the solvent refractive index. DLS uses an average particle size approach that has an intensity bias towards larger particles that may be contaminants in the sample. Given this intensity bias, DLS requires a high concentration of particles in order to achieve higher light scattering. The working concentration range for NTA is 10^6 – 10^9 particles per ml, depending on refractive index and particle size (Panalytical). Applications of these techniques includes structural studies, development of drug delivery systems, viral vaccine development, nanotoxicology, protein aggregation studies, and extracellular vesicles characterization (Filipe, Hawe and Jiskoot; Vestad et al.).

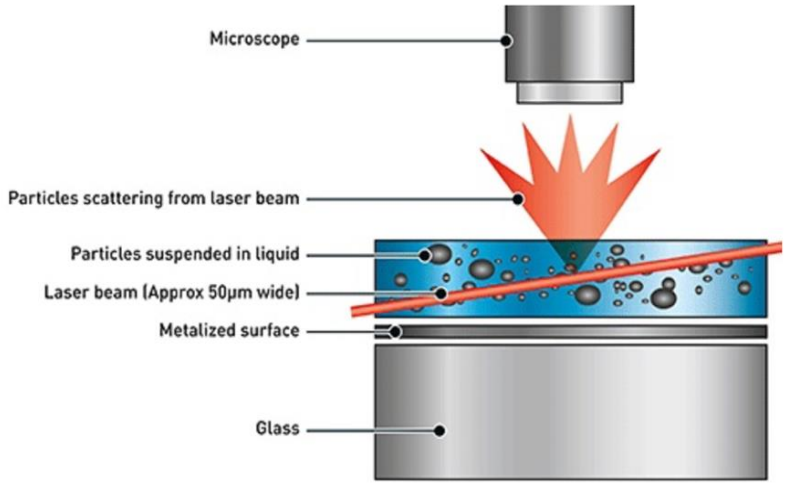

Figure 12. Schematic of Configuration for NTA [Panalytical]

b. EM-Negative staining & Cryo-EM-vitrified samples

The electron microscope uses radiation in the form of electrons. Imaging biological structures by electron microscopy was demonstrated in 1975 by Henderson et. Al. who achieved a 7Å resolution map of tilted, unstained specimens of bacteriorhodopsin (Henderson and Unwin). This led to progress in attaining atomic resolution structures for many icosahedral viruses. High resolution structures have been attained for non-organic samples which can tolerate high electron doses unlike organic materials. This is due to the ability of the non-organic samples to be imaged with high doses of electrons without losing structural integrity. This is the challenge in imaging proteins, viruses, and cells; the sample endures extensive damage from electron irradiation causing breakage in chemical bonds (Milne et al.).

In order to attain better contrasting images, the negative staining was employed. Negative stain surrounds the sample making an inverse contrast replica of the sample.

The heavy metals contain a high number of electrons that interacts with the electron beam to produce contrast. There is a trade-off of internal structural information and the possibility for artifacts when using UA staining. Another possibility for reducing the damage to the sample is to use lower electron doses, but this yields images with poor-signal-to-noise ratio due to the unstained sample being made up of low atomic number elements that scatter electrons poorly (Milne et al.). Consequently, the issue that arises in imaging of unstained sample is that electron doses low enough to reduce radiation damage generates noisy images, while high electron doses lead to high amounts of specimen damage (Milne et al.). To remedy the situation a large number of these images can be averaged to produce images of each atomic position. This is the fundamental difference between XFEL which uses a really high dose but a femtosecond pulse, before the molecules is completely ionized, and cryoTEM which uses really low dose and many thousands of images averaged.

Cryo-electron microscopy (cryo-EM) over the years has become a popular technology for studying cells, viruses and proteins at a high resolution on a molecular scale (Glaeser and Hall; Milne et al.). Cryo-EM is a technology that utilizes a transmission electron microscope to image specimens under cryogenic conditions (Fig. 13). Samples for this technique remain hydrated and are cooled to cryogenic temperatures in the absence of ice (Fahy and Wowk).

There have been large strides in the cryo-EM field that have led to developments in the microscope design and imaging hardware (Molineux and Panja). These developments have significantly improved the resolutions achieved by this technology.

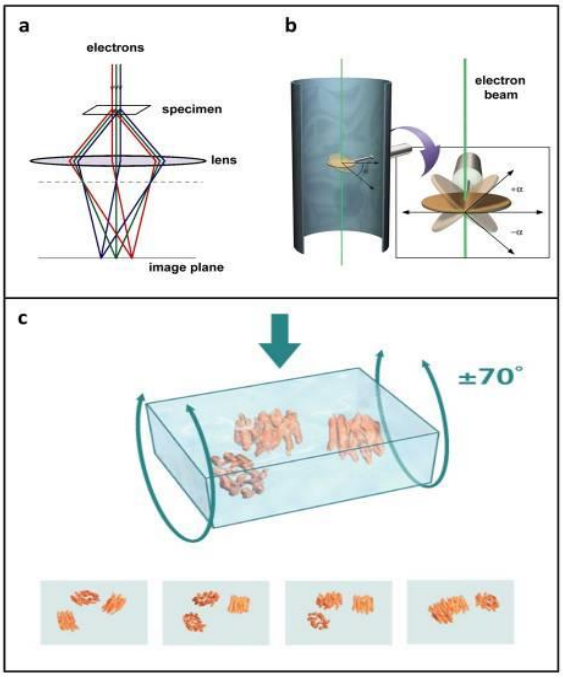

Figure 13. Image Formation by Electron Microscopy and Cryo-EM Tomography [Milne].

Cryo-EM samples must be maintained at liquid nitrogen or helium temperatures for imaging to be performed. Studies have shown that cryogenic conditions reduce the amount of radiation damage caused by using high electron doses as opposed to room temperature conditions (Glaeser). Samples are plunge frozen into a cryogen, such as liquid ethane, which is cooled by liquid nitrogen (Glaeser). This methodology is employed to prepare samples for cryo-EM tomography, single-particle imaging, and crystals. Cryo-EM tomography is a technique used to collect a series of images at different orientations relative to the electron beam (Milne et al.). The images collected can be combined using computer programs to generate 3D images of the sample. This tomography technique has provided insight into a variety of areas regarding the bacterial cytoskeleton, DNA ejection in Bacillus anthracis spore-binding phage and cell-cell fusion

(Fu et al.; Kudryashev et al.; Lech, Reddy and Sherman). Single particle cryo-EM is another technique employed to generate a 3D structure. A large number of 2D projections are taken that are identical copies at different orientations, which are combined to produce a 3D reconstruction of a structure. To begin carbon grids are glow discharged, and specimen is added to the surface of the grid and evenly spread. The grids are glow discharged long enough to allow the water to spread so that a vicinal film will form. The grid is plunged into liquid ethane that is cooled by liquid nitrogen, creating a thin sheet of vitreous ice. The grid(s) are loaded onto the cryo-EM. Ice thickness can vary across the grid, meaning that certain areas may have sufficient or insufficient thickness to produce quality images.

The areas and single particles that are selected for imaging may be chosen manually or by automated algorithms (Milne et al.). Chosen particles within the dataset are then sorted and processed using different statistical methods and computer programs based on structural features (Milne et al.). The relatedness of the individual particle images is used to cluster similar images within a data set (Vénien-Bryan et al.; Milne et al.) These images are averaged to create characteristic projection views allowing for visualization of finer structural features at high signal to noise ratio (Milne et al.). 3D reconstruction is dependent on the relative orientation of all the particles and involves the central projection theorem (Fig. 14). Fourier transform is an image processing tool used to perform the operation of merging 2D projections into a 3D (Fig. 14).

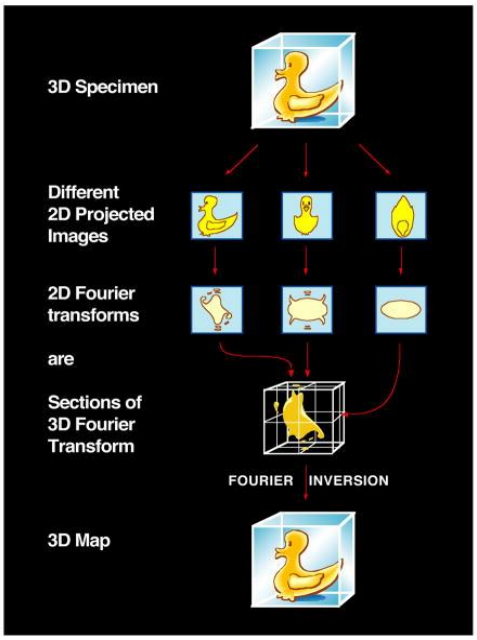

Figure 14. Fourier Inversion 3D Reconstruction [Milne] .

Acquiring large amounts of images comprising different orientations in respect to the electron beam can be used to build 3D reconstructions (Milne et al.; Vénien-Bryan et al.). The overall workflow for 3D single particle reconstruction using cryoEM can be seen below (Fig. 15).

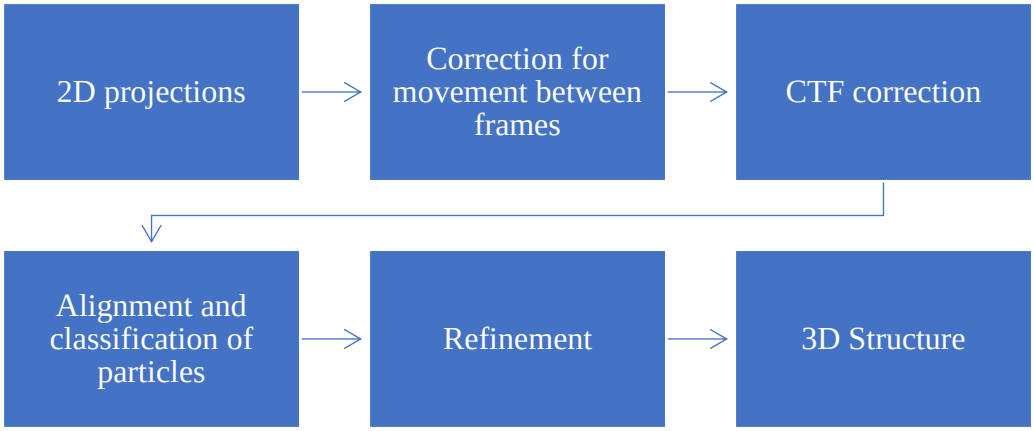

Figure 15. Flow Work of 3D Single Particle Reconstruction.

Data is initially collected as a series of projections that are a random orientations within the vitreous sheet (Vénien-Bryan et al.). Alignment and classification of the 2D projections as well as refinement of the orientations is performed before the 2D projections are combined to yield a 3D structure (Vénien-Bryan et al.).

The single particle approach has proven to be successful for solving icosahedral virus structures. Some of the highest resolution achieved using this approach has been for imaging icosahedral viruses. Factors that account for this success are high symmetry and size of the virus particles. The high symmetry is helpful in averaging the virions and the large size of the virions allow for high contrast leading to ease in determining particle orientations in projection images (Milne et al.). Furthermore, there have been numerous of advancements in a variety of parameters that are essential for structural discovery using cryo-EM. Advancements in transmission EM, detectors, and image processing software have led to higher resolution achievements (Renaud et al.). The advancements in detectors include the changing from photographic film to charge-coupled device (CCD) cameras to direct electron detectors. Images are usually recorded as stacks of 'movie frames' (Renaud et al.). Lastly improvements in software algorithms and computational hardware utilization has efficiently delivered high resolution 3D structures. Submissions to the Electron Microscopy Data Bank (EMDB) using the single-particle method, have resolutions in the range of 2–5 Å ("Challenges for Cryo-EM").

Cryo-EM has the capability of solving structures at high resolutions thanks to the automation of data collection and the advanced algorithms for model building and reconstructions. This technique does not require large amounts of sample, instead it

requires a low volume of high concentrated sample. Samples used for cryoEM can show a variety of conformational states. This heterogeneity can reduce the resolution that can be achieved but allows for the modeling of dynamics and conformational transitions which can provide insight on biological functions (Vénien-Bryan et al.). This is done by classifying the images into different classes that represent the different conformational states (Vénien-Bryan et al.). Although cryoEM is a technique that offers solving structures at very high resolutions it does have several challenges and limitations that have to be worked through. These challenges include low signal to noise ratio or low contrast which limits the size that can be observed.

c. XFEL

XFEL is a developing technique used to solve 3D structures of macromolecules. Unlike cryoEM the experiments conducted utilizing the XFEL are done at room temperature. The XFEL utilizes electron pulses which are accelerated until they reach a very high energy and the speed of light. The electron pulses pass between a row of alternating magnets which causes lateral undulations resulting in the release of X-rays. Interactions between the electrons, X-rays and their alignments create a coherent or laser light that results in increased energy of the X-ray pulses (Johansson et al.). The X-ray laser pulses continue to the experiment hall to the interaction region. The interaction region is defined as the area where the beam and sample (crystals or single particles) interact to produce a diffraction pattern. The X-ray pulses are measured in femtoseconds which is a quadrillionth (10^{-15}) of a second (Johansson et al.). X-ray pulses at the first generation XFEL at LCLS I delivered pulses at ~120/sec. X-rays damage samples such as

viruses and crystals, but the brief pulses produced by the XFELs “outrun” radiation damage so high-resolution, room-temperature structures can be determined, as well as time resolved and dynamic imaging to capture real-time biological processes (Fig. 16).

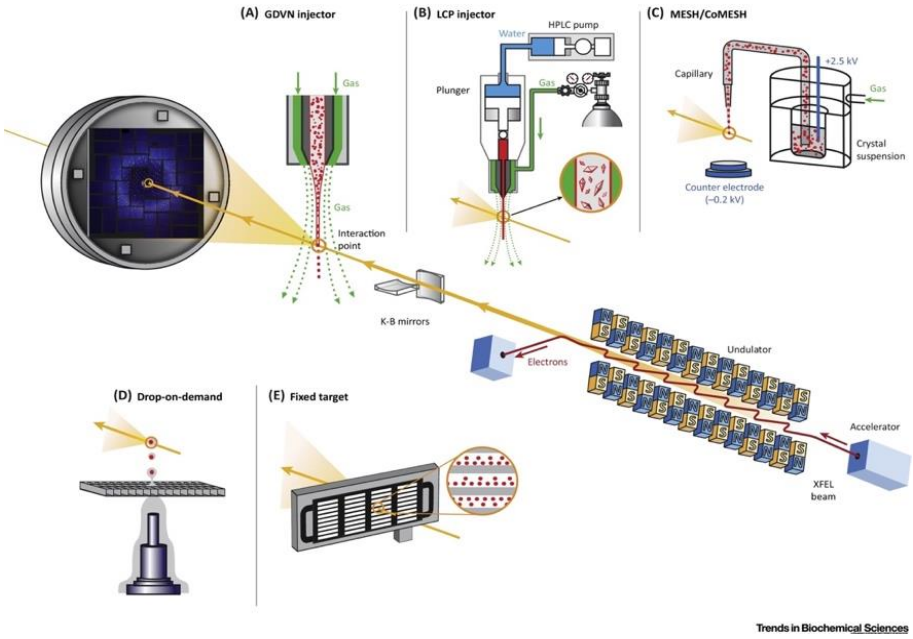

Figure 16. Schematic of XFEL Beam Delivery [Johansson]

There are a variety of ways that sample can be introduced to the beam (Fig. 16). For the purposes of this thesis and experimental design method the gas dynamic virtual nozzle (GDVN) injection was used (Fig. 17).

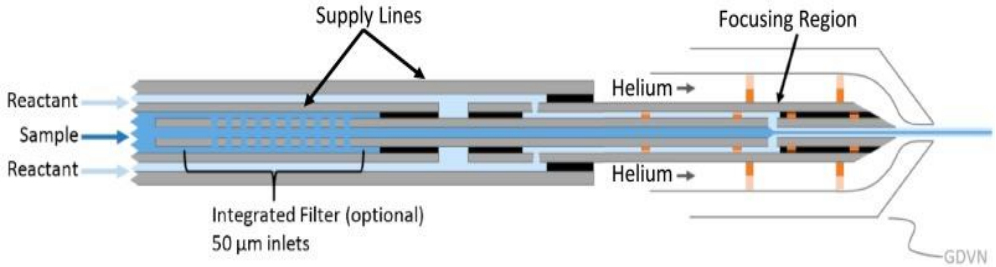

Figure 17. Schematic of GDVN Injection System [Calvey et al.].

This methodology employs the use of a high-pressure gas in order to create a micron scale liquid jet that is held at low flow rates (μL/min) (Calvey et al.). Initial equilibration of equipment such as injectors, detectors, etc. is done before sample loading and data collection. A large multidisciplinary team comes together to conduct these experiments and the XFEL monitoring during the experiment is done by the beam scientists.

XFEL diffraction experiments generate a large quantity of data at the FEL repetition rate (Andreasson et al.). The data collected can contain hits on single particles, clusters and contaminants (Andreasson et al.). Identification of useful diffraction data can be sorted into different classes. A hit finder tool is used to effectively identify particle hits. Screening of the large amounts of data generated by the XFEL can be difficult, but the use of computational algorithms allows for faster and efficient screening. The work flow for image processing consists of (i) hit- finding, data picking; (ii) data sorting; (iii) recovering orientations and volume merging; (iv) phase retrieval for 3D modeling; (v) 3D model refinement (Liu and Spence).

There are several XFEL facilities all over the world which include: LCLS I and LCLS II, the latter is currently under construction (USA), SACLA (Japan), European XFEL (Germany), PAL-XFEL (South Korea), SwissFEL (Switzerland). There are few of these facilities since the cost is large. The construction of the European XFEL that opened in 2017 was approximately 1.22 billion euros. The Linac Coherent Laser Source (LCLS I) was the XFEL used for the experiments described in this thesis. At the LCLS there are several hutches in which the instrumentation is designed for specific

experimental purposes. For the purposes of the set of experiments described the Atomic, Molecular & Optical Science (AMO) hutch at the LCLS was utilized.

CHAPTER 3

MATERIALS AND METHODS

i. Plates and Buffers

Recipes for all buffers used for the propagation and purification of PR772 are listed in Table 1. All buffers were set to a pH of 8.0 and passed through a 0.22μm Millipore filter. The filtration is necessary per instruction manual given by the manufacturer of the AKTA FPLC. The overlay method was used to propagate PR772. Both layers have Tryptic Soy Broth (TSB) but differ in their composition of agar (Table 2). The bottom and top layers are composed of 1.5% and 0.5% agar, respectively.

Table 1. Buffers used throughout PR772 Propagation and Purification

Ingredient	**Elution Buffer A**	**Elution Buffer B**	**Start Buffer**	**Storage Buffer**	**3X PEG**
Tris	50mM	50mM	50mM	50mM	N/A
NaCl	N/A	1.5M	100mM	100mM	17.4% W/V
$MgSO_4$	1mM	1mM	1mM	1mM	N/A
EDTA	N/A	N/A	N/A	1mM	N/A
PEG 8,000	N/A	N/A	N/A	N/A	27% W/V
PEG 20,000	N/A	N/A	N/A	N/A	N/A
DI Water	**Fill to 1L**	**Fill to 1L**	**Fill to 1L**	**Fill to 500mL**	**Fill to 500mL**

Table 2. Plate compositions

Type of agar	**Soft agar overlay**	**Hard agar**
Tryptic Soy Broth (TSB)	6g	15g
Agar (% w/v)	0.5%: 1g	1.5%: 7.5g
DI water	**Fill up to 200mL**	**Fill up to 500mL**

ii. *E. coli* Stocks

E.coli K12 J53-1 (ATCC BAA-769) pellet was rehydrated with 1.0 mL of TSB and added to flask containing fresh TSB. The culture was incubated overnight at 37°C while shaking at 220 rpm. The *E.coli* was then isolated using the isolation streak method, as indicated in Figure 18 and incubated overnight at 37°C.

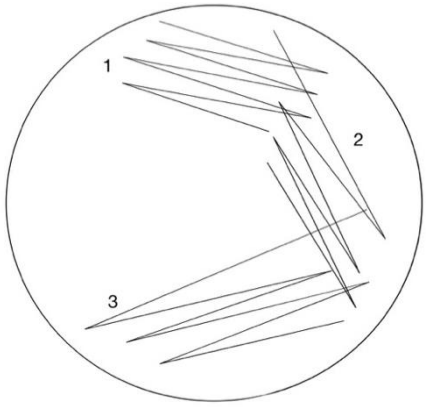

Figure 18. Isolation Streak Schematic.

Several colonies were picked and incubated overnight with 5 mL of TSB at 37° and shaking at 220 rpm. This was then aliquoted into volumes of 500 μL with 500 μL of 30% glycerol added. These aliquots were then put into the -80°C freezer for storage.

iii. Rehydration and Enumeration of PR772

Enumeration of PR772 (ATCC BAA-769-B1) was done to check virus viability and titer. A few microliters of *E.coli* stock were placed into fresh TSB and incubated overnight at 37° C in a shaker at 220 rpm. The following day 15 mL of fresh TSB was inoculated with 2 mL of the overnight culture and incubated at 37° C and shaking at 220 rpm for about 1-2 hours to reach an OD_{600}=0.7. To prepare virus stocks the overlay method. The inoculum was added to 50 mL of soft agar and mixed, before pouring over the hard layer and allowed to solidify. Resuspended PR772 was serially diluted (10^{-1},10^{-2},10^{-3},10^{-4},$10^{-5\cdots}10^{-10}$) by adding 0.5mL of the phage into 4.5mL of fresh TSB. A plaque assay was performed to determine the titer of the sample, 50 µl of the phage was placed into 450 µl TSB, and the dilution series was increased to 10^{-15}. The dilutions were spotted onto the overlay (Fig. 19). The spotting was done in duplicate to assure accuracy. The plates were incubated at 37 ° C for about 18 hours, at which time the lysis was visible. The plaques were counted, and the titer was calculated.

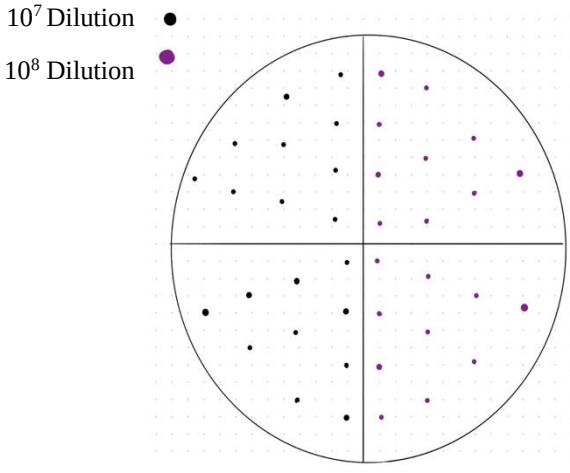

Figure 19. Plaque Assay Schematic

iv. Viral Stocks

A few microliters of *E.coli* stock were placed into fresh TSB and incubated overnight at 37° C, 220 rpm. The following day 2 mL of suspension was added to 15 mL of TSB and incubated at 37° C with shaking at 220 rpm and grown to mid log phase. For the infection 1 ml of 10^8 pfu/mL of PR772 was added to 9 mL of mid-log-phase bacteria and incubated for 5 min at 20 to 25°C. This suspension was added to the cooled soft agar and 7-8 ml of the mixture was poured onto the surface of 100-mm-diameter tryptic soy agar plates. The plates were allowed to solidify before incubation overnight at 37°C, allowing lysis of the bacterial lawn by PR772. After approximately 18 hours, the overlay was scrapped off the agar plates into a sterile container containing 40 mL of 1X storage buffer and mixed overnight at 4 °C. The mixture was centrifuged at 8,000 x g for 30 min and the supernatant was filtered through a 0.22 μm Millipore filter. The filtrate was tittered and stored at -80°C. The titer of the stock was measured as 3.5 x 10^{10} pfu/ml.

v. Virus Propagation

10 mL of TSB was added to an Erlenmeyer flask with several μL of *E. coli* stock and incubated overnight at 37° C with shaking at 220 rpm. The following day a secondary flask was inoculated with 200 μL of overnight culture and 20 mL of fresh TSB. This culture was incubated at 37°C and shaking at 220 rpm for about 1-2 hours to reach mid-log-phase. Hard agar plates (25, 100mm plates) were warmed in a 37°C incubator. Soft agar was melted by microwaving and allowed to cool in a water bath at 45°C. *E. coli* (OD_{600}=0.5) and viral stock (3.5 x 10^{10} pfu/ml) were mixed together and

incubated for 5 min. This mixture was added to the soft agar in a volume ratio of 10:1:200 (mL) and 7-8 mL was poured onto the hard agar dishes. Plates were inverted once solidified and incubated overnight at 37° C for 16 h.

vi. Polyethylene Glycol (PEG) Precipitation

PEG precipitation was used to concentrate PR772 after growth in the soft agar. The soft agar layer was scraped into 7 mL of sterile 1X storage buffer and mixed for 4 h at room temperature. The mixture was centrifuged at 8,000 x g for 30 min and the supernatant was filtered through a 0.45 μm filter. The filtered supernatant was placed into a clean centrifuge bottle and 3X PEG (Table 1) was added in an amount to give a final PEG concentration of 1X (PEG 9%, NaCl 5.8%). This was mixed and incubated overnight with rocking at 4°C . The mixture was centrifuged for 1.5h at 4°C and 8,000 x g. The pelleted virus was resuspended into 2 mL of 1X storage buffer and incubated overnight while rocking at 4°C.

vii. Ultracentrifugation

Soft-top layer was scraped off into a sterile container containing 7 mL of 1X storage buffer and mixed for 4 hours at room temperature. The mixture was centrifuged at 10,000 x g for 15 min and the supernatant filtered through a 0.45 μm filter. The filtered supernatant was placed onto a cushion of 80% sucrose and ultracentrifuged for at 4°C at 90,000 x g for 2 h. A thin blueish band corresponding to virus was then extracted using a needle and syringe. Approximately 4 mL of 1X storage buffer was added to equilibrate the sample to 100 mM salt concentration and lower the viscosity prior to injecting the sample onto a CaptoQ column without affecting FPLC pressure.

viii. Purification

A 5 mL HiTrap CaptoQ (GE Healthcare) anion exchange column was equilibrated with several column volumes (CVs) of start buffer prior to loading (Fig. 20, Table 1). The virus was loaded onto the column and injected at a flowrate of 1mL/min. Start buffer was run through the column until the UV absorption zeroed and was stable. After UV stabilization the sample was eluted with a step gradient using high salt concentration elution buffer (Table 1). A single peak was collected.

Figure 20. HiTrap CaptoQ Anion Exchange Column (GE Healthcare) Utilized for Purification

ix. PD MiniTrap G-10 Desalting Columns

The single virus peak eluted with 20% of the 1.5 M NaCl elution buffer. In order to remove excess salt and bring the salt down to 100mM, a buffer exchange was done using mini PD-10 desalting columns (GE healthcare). The column was equilibrated with 8mL of 1x storage and 0.3mL of purified virus was put through with an additional 0.4mL of 1x storage buffer (Fig. 21, Table 1). The sample was eluted out with 0.5mL of 1x storage buffer. The 100 mM final sample was used for further characterization.

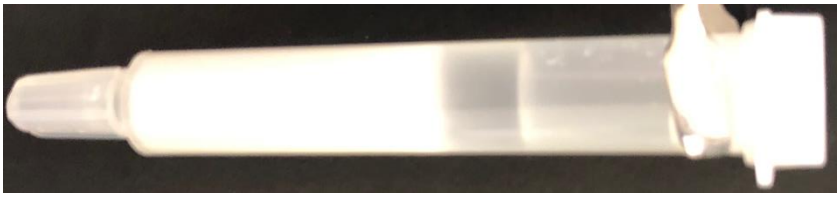

Figure 21. PD MiniTrap G-10 Desalting Column (GE Healthcare) Utilized for Buffer Exchanging Virus Sample.

x. PEG-20 Concentration

Pierce™ Slide A Lyzer® MINI Dialysis Units, Thermo Scientific, were used to concentrate the virus after desalting. The dialysis unit was washed thoroughly with DI water before being placed in a 2 mL centrifuge tube filled with PEG-20. Virus was added to the dialysis unit and incubated on ice for several hours, with constant monitoring so that the sample did not completely pass through the membrane.

xi. Characterization: Nanodrop Reading

Nanodrop readings at OD_{280} were used measure the concentration of the virus following the PEG-20 precipitation step.

xii. Viral Enumeration-Plaque Assay

Plaque assays were used to determine the titer of the concentrated infectious virus. TSB (10 mL) was inoculated with several μL of *E. Coli* stock and incubated overnight at 37°C in a shaker at 220 rpm. The following day 20 ml of fresh TSB was inoculated with 200 μL of the overnight culture. The culture was incubated at 37°C with shaking at 220 rpm for about 1-2 hours to reach mid-log-phase, OD_{600}=0.6. Hard agar plates (25, 100mm plates) were warmed in a 37^{o}C incubator. The soft agar overlay was melted in the microwave and equilibrated in a water bath. *E. coli* and soft agar were

mixed, poured onto the hard agar plates and allowed to solidify. The virus sample was serially diluted (10^{-1},10^{-2},10^{-3},10^{-4},$10^{-5\cdots}10^{-10}$) by adding 10μL of virus to 90μL of fresh TSB. Each dilution was spotted in duplicate on the surface of the overlay. Plates were incubated at 37°C overnight, plaques were counted, and the titer calculated.

xiii. Cesium Chloride Step Gradient

A cesium chloride (CsCl) step gradient was implemented as an additional purification step. This step was implemented to separate damaged and intact particles. The CsCl step gradient was prepared using the following equation (Lech, Reddy and Sherman), with ρ equaling density:

$$137.11 - \frac{138.48}{\rho}$$

Two densities were used in the step gradient: 1.34g/cm^3 and 1.7g/cm^3. Each were prepared and added to an ultracentrifuge tube. Two milliliters of the 1.7g/cm^3 density solution was added to the tube then the 1.34g/cm^3 density solution was gently layer on top. The virus sample was gently layered on top, care was taken not to mix the sample with the dense solution. The tube was added to the SW41 Rotor Ti swinging bucket holders (Beckman Coulter). The holders were balanced and loaded onto the rotor. Ultracentrifugation was then completed at 4°C, 100,000 x g for 2 h. The resulting bands were extracted, and buffer exchanged as previously described.

xiv. NanoSight Measurements

PR772 viral preps were diluted to approximately 10^8 particles in 1X storage buffer for NanoSight (Malvern NanoSight NS300) measurements of particle size distribution and concentration.

xv. Electron Microscopy

Purified virus was visualized by negative staining and EM (Fig. 22) (Meister and Blume). Formvar/carbon coated grids were (Electron Microscopy Sciences, West Chester PA.), stabilized with evaporated carbon film. These grids were spotted with 5µL of sample and incubated for 2 min. Excess sample was blotted with filter paper and grids were negative stained with 5 µL of 2% uranyl acetate. The excess stain was blotted, and the grids were rested on filter paper to air dry. Stained grids were loaded onto a Tecnai F20 (Phillips Corp, NL) transmission electron microscope (TEM) for visualization.

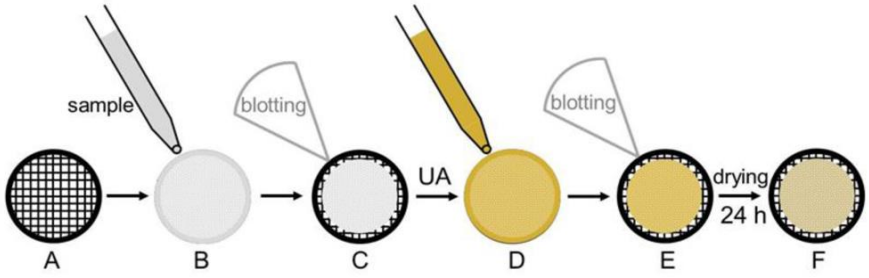

Figure 22. Schematic of Negative Staining Procedure [Meister and Blume].

xvi. Cryo-EM Sample Vitrification Preparation

Sample that appeared to have whole viral particles and lack background impurities was plunge frozen using holey carbon grids. Grids used for cryoEM were the C-Flat™ Holey Carbon Grid (Protochips, Research Triangle NC.), CF-2/1-4C, Hole Size=2.0 µm, Material=Copper, Spacing=1.0 µm, Mesh=400. The grids were glow

discharged on each side for no more than 15 seconds. Glow discharging the surfaces of the grids allowed them to become hydrophilic. The grids were loaded onto the Vitrobot and sample was added 3μL at a time. The excess sample was blotted of and additional sample was added.

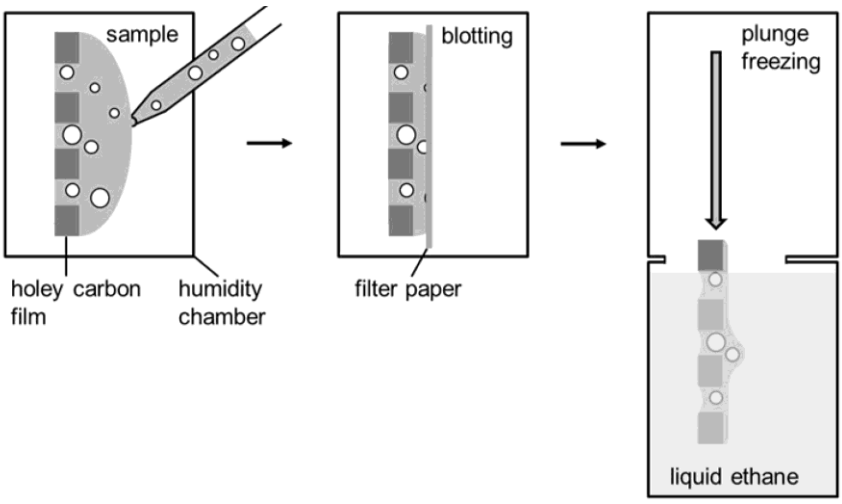

Figure 23. Schematic of Plunge Freeze Procedure [Meister and Blume].

This was repeated 2-3 times before the grid was plunged into liquid ethane cooled by liquid nitrogen (Fig. 23) (Meister and Blume). The sample was loaded onto a cassette for storage and stored into liquid nitrogen. The prepped grids were taken to the FEI Titan Krios (FEICO, Hillsboro OR.) for further screening and imaging.

xvii. Imaging

Imaging was performed at nominal magnification of 18,000K, which gave a 0.68-pixel size on the K2 Summit camera (Gatan Pleasantville, CA) in super-resolution mode. Each image consisted of 40 frames taken over an 8 second exposure time with an electron flux of 2 e^-/pixel*second.

xviii. Image Processing

All image processing was performed in cisTEM (computational imaging system for transmission electron microscopy)((Grant, Rohou and Grigorieff), including motion correction, CTF determination, and reconstruction. A total of 1,249 images were motion corrected and 3,612 particles of PR772 extracted. After 2D classification 302 particles were used for reconstruction of a 3D volume of PR772. Final resolution by 0.5 FSC was 11 Å.

xix. Storage

Virus was stored in 1X storage buffer at 4°C. . Several virus preps were negative stained at different time frames (2 weeks, 1 month, 2 months, 3 months) to observe any changes while “aging” at 4°C.

CHAPTER 4

RESULTS

i. Purification Results: FPLC profile

Following the initial pre-purification and concentration steps, FPLC was used to purify PR772. The concentrated virus from twenty-five 100 mm plates was bound to HiTrap CaptoQ (GE Healthcare) anion exchange columns in storage buffer (50 mM Tris, 100 mM NaCl, 1 mM MgSO4 and 1 mM EDTA, pH 8.0). The virus was eluted with a step gradient (0-1.5 M NaCl) and pressure held at 0.1-0.17 MPa. UV absorbance, conductivity and pressure were monitored (Fig. 24).

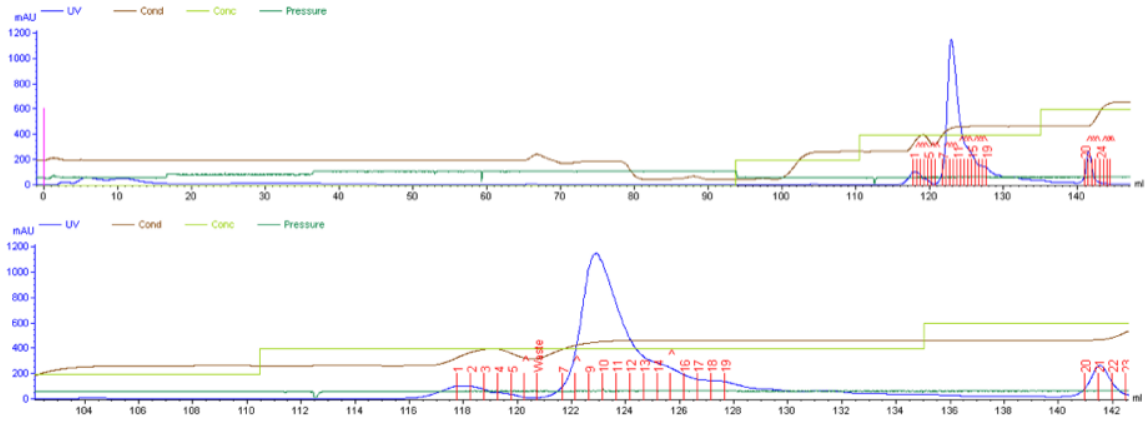

Figure 24. FPLC Chromatogram.

PR772 typically eluted at 20% of 1.5 M NaCl (300 mM) as a single peak with a shoulder (Fig. 24). UV absorbance measured between 700-1100 mAU. Two additional small peaks with low absorbance were also observed. Material from the small peak that eluted after the virus was imaged and significant background that contained pili-like structures was observed (Fig. 25).

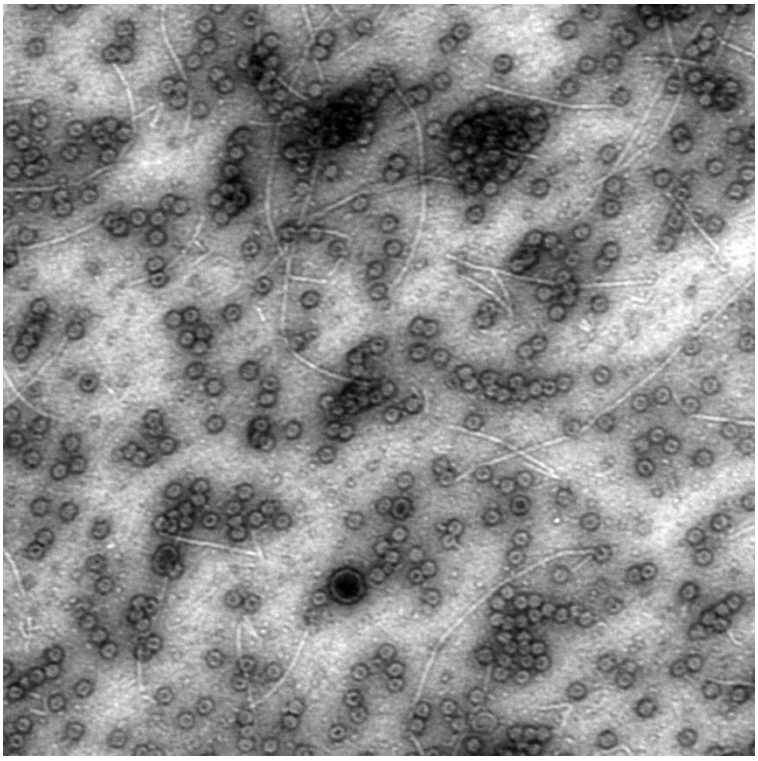

Figure 25. PR772 Virus Fraction with Pilli-like Structures and Dirty Background

The chromatogram was adjusted to show the fractions within the sharp peak, allowing for collection of a high concentration, clean fraction (Fig. 24 bottom panel).

ii. Characterization Results

a. Viral Enumeration: Plaque Assay

To determine how much infectious PR772 virus was present in the FPLC fractions, plaque assays were used. The spotting method was used. Different dilutions of the purified virus were spotted onto a lawn of bacteria (Fig. 26). Dilutions were spotted in duplicate. The virus yields were typically around 2.25×10^{12} pfu/mL.

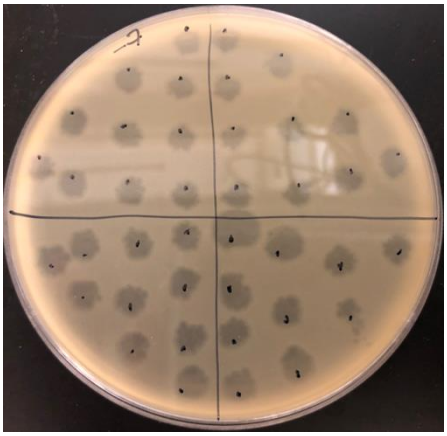

Figure 26. Plaque morphology.

b. NanoSight

NanoSight measurements were also taken to determine the concentration and size distribution of purified PR772 (Fig. 27). The virus exhibited a sharp peak for a ~71nm size particle, consistent with the expected size. The NanoSight concentration measurement of 1.52 x 10^{12} particles was similar to the plaque assay measurement.

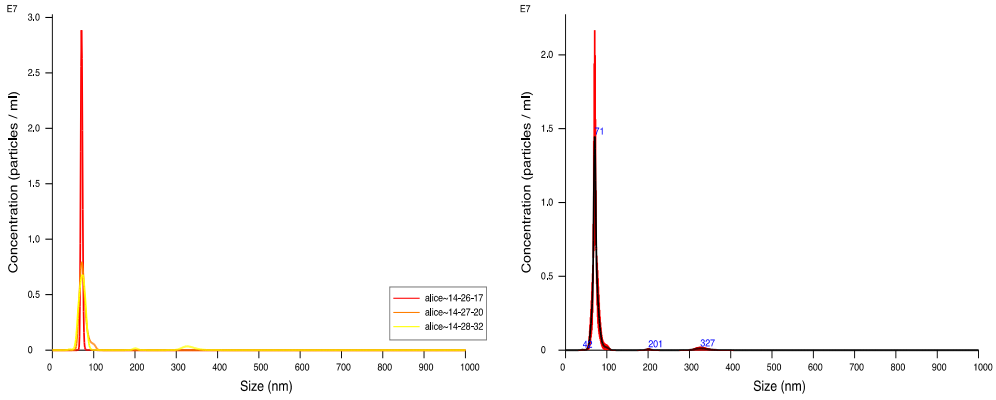

Figure 27. NanoSight Virus Size Distribution Profile.

c. Electron Microscopy

EM was used to further confirm the concentration of virus preps and to check the integrity of the particles. Following purification and the final buffer exchange, virus was spotted on formvar/carbon coated stabilized grids and negative stained with 2% uranyl acetate (UA). Images were taken at a low magnification to show the dispersed particles and give an idea of the concentration and purity (Fig. 28).

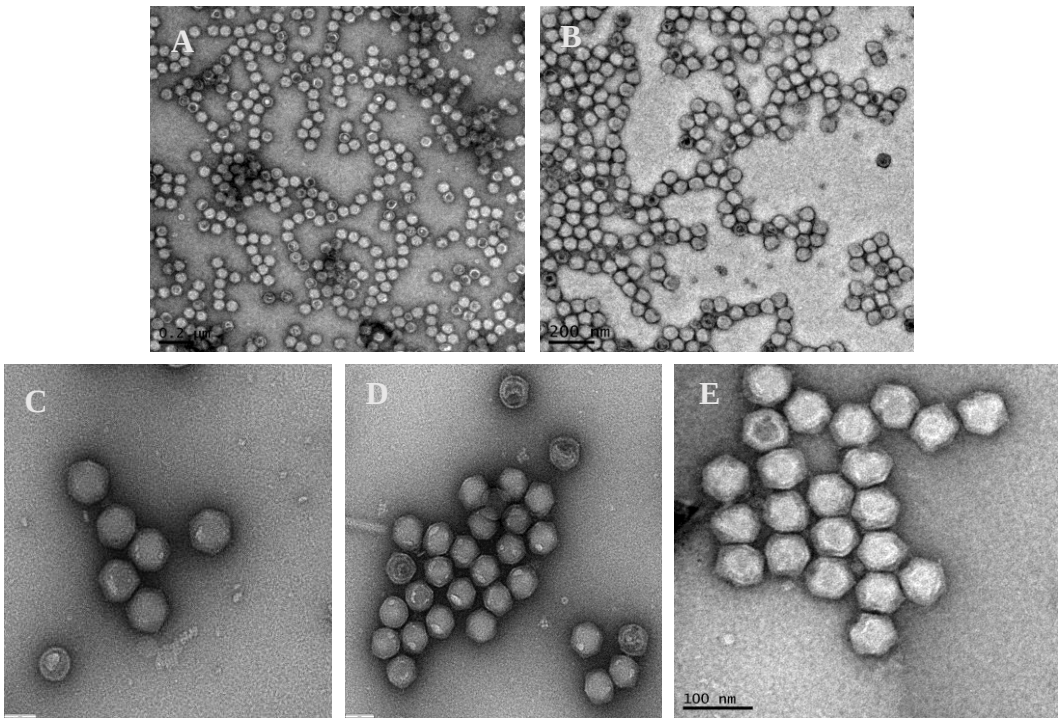

Figure 28. Negative stain PR772 Visualization with Screening TEM.

Lack of background and pili-like structures show that the viral sample was clean and adequate for XFEL experiments or plunge freezing for Cryo-EM. A majority of the particles exhibit icosahedral structure with an inner lipid membrane. Individual particles

were also imaged at a higher magnification; the exclusion of stain from the viral capsid interior demonstrates the presence of the genome and an intact capsid (Fig. 29 C-E).

iii. SPI X341 XFEL Experiment Results

SPI experiment X341was done with the purpose of achieving a higher resolution structure for PR772. PR772 samples prepared as described were used for the beamtime that consisted of 4 shifts in September 15-19, 2018 at the LCLS AMO end station. The beamtime results below are based on summaries provided by the beam scientists at the end of each shift.

Shift I

During the first shift apertures and detectors were quickly aligned in the first 2h, but it was noted that 2 of 8 readout channels on the PNCCD detector were not working. Having a fully functional detector is important to obtain the highest possible resolution. The beam scientist indicated that resolution is limited to ~2.5 nm at the edge when 1 panel is lost. A significant amount of time was spent with the detector team diagnosing and trying to fix the panels, but with ultimately no success. Late in the shift, a decision was made to move forward with sample injection. Weak single particle hits were initially seen. Analysis of the problem found that the KB mirror focus was ~12 cm off-center of the sample chamber. After correcting the alignment, strong hits were detected, but the hit rate remained low. It appeared that the system was clogged since the flow rated was ~1/4 or less than expected. It was hypothesized that the PR772 concentration was too high.

Shift II

Attempts were made to fix the PNCCD detector panels between the first and second shift. This was not successful, and the experiment was continued with the missing tiles. After cleaning the skimmer and optimizing the injector jet, very good single particle hits were collected for ~4 h. The high rate remained at 1%.

Shift III

At the beginning of the third shift nozzles were changed and data collection began and continued without problems for the remainder of the time. The hit rates were ~1%, with ~1/3 of the hits being single particles. The remaining hits consisted of PR772 surrounded by a water layer and clusters of particles.

Shift IV

At the beginning of the fourth shift the nozzle stopped jetting. The nozzle was changed, and the helium flow was increased, which resulted in good flow and a hit rate of ~2% and increased single particle diffraction patterns. Fewer particles were surrounded by water as was seen the previous day.

Beamtime X341 Summary

The data from the X341 beamtime is still being analyzed by multiple SPI subgroups, but a preliminary report during an initial data analysis meeting in December 2018 indicated that from 197,667 processed patterns, only 1,393 were single hits (SPI unpublished preliminary analysis). Examples of the diffraction snapshots collected are shown in Figure 29.

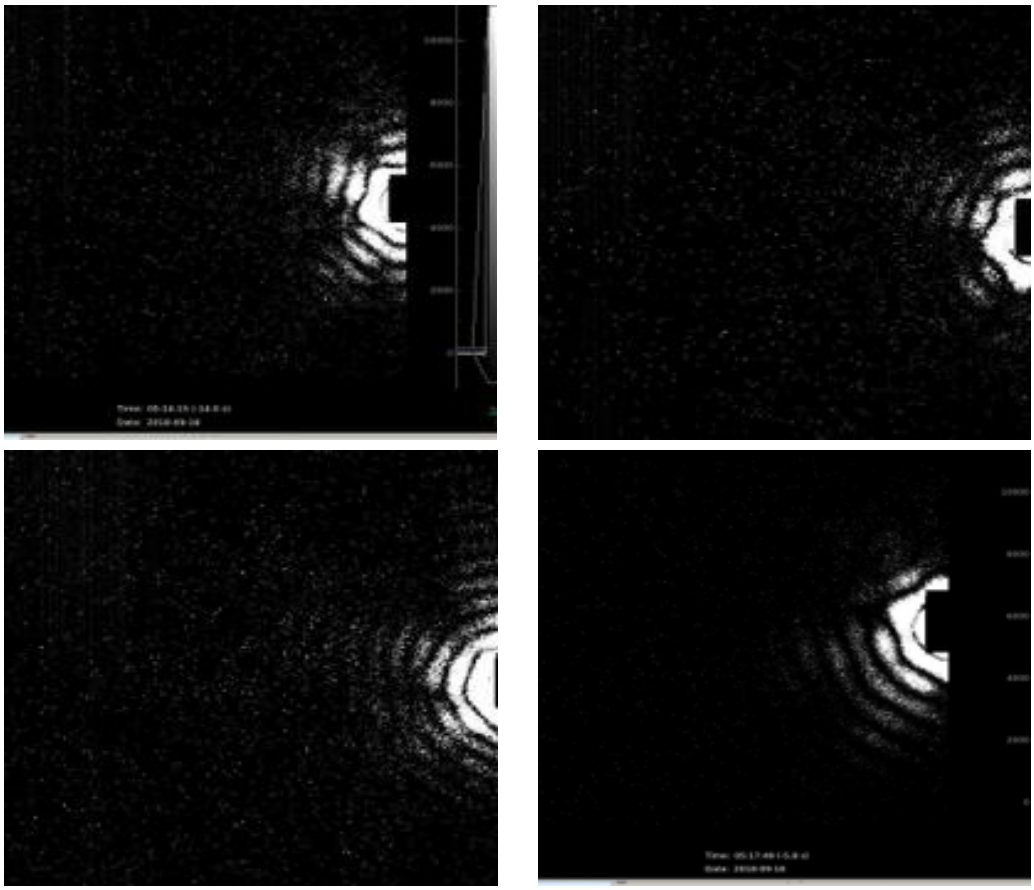

Figure 29. Diffraction Snapshot Patterns for PR772.

The preliminary data analysis for X341 indicates that some diffraction patterns extended to 7nm (SPI unpublished preliminary analysis). This is encouraging since the highest resolution achieved for PR772 in the previous SPI beamtimes was 9nm (Hosseinizadeh et al.). However, the low number of diffraction patterns at 7nm will likely not be sufficient to generate a high-resolution 3D structure. Further analysis of the full data set will provide a more definitive picture of information gained from the X341 beamtime. Since PR772 was shot during multiple SPI beamtimes, the team may pool the data from all of these, with the hope that analysis of the larger collective data set might collectively yield

sufficient higher resolution information from which a higher resolution 3D reconstruction can be generated.

iv. Cryo-EM Results

As a complementary approach and with the goal to obtain a higher resolution structure, PR772 preps were also imaged by cryoEM. Krios imaging and data processing for PR772 was done by Dewight Williams of the John M. Cowley Center for High Resolution Electron Microscopy (CHREM). After determining that a virus prep was adequate, samples were plunge frozen. Frozen samples were imaged with the Titan Krios (FEI) in the John M. Cowley Center for High Resolution Electron Microscopy (Fig. 30).

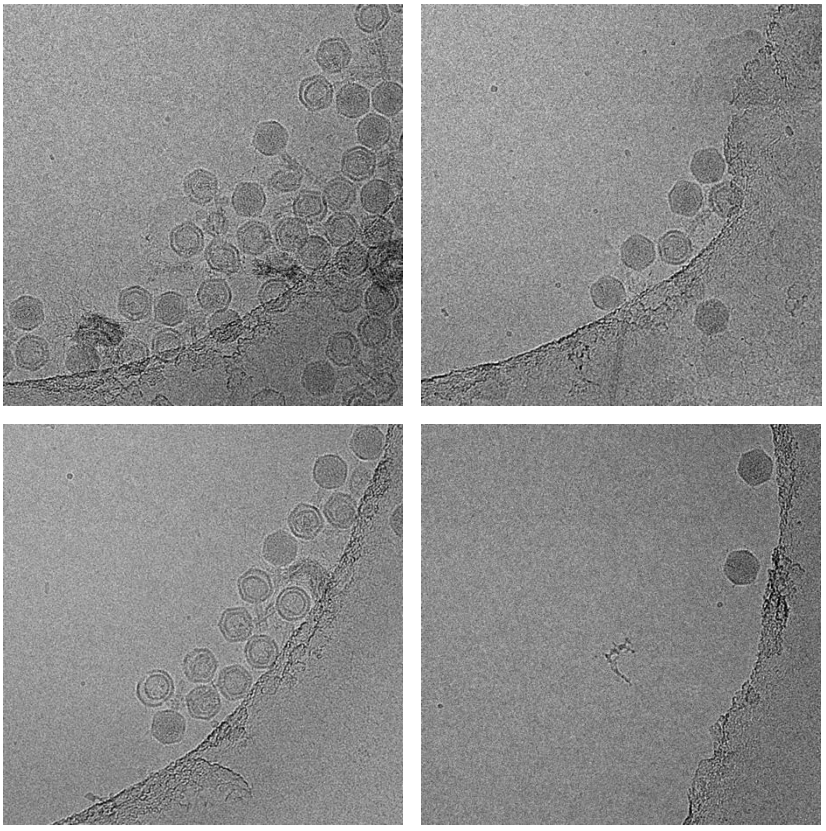

Figure 30. Krios Images of PR772 Viral Particles.

A heterogeneous population of particles were present in the frozen samples. This was unexpected since the negative stained screens of the prep showed a more homogeneous spread of viruses. The frozen samples appeared to have been damaged during the plunge freezing, with some appearing to have lost their genome and some exhibiting nanotube-like structures. Since the frozen preps exhibited significant heterogeneity, single particle images were manually selected and classified based on variations in their structural features. These images are averaged to create characteristic projection views allowing for visualization of structural features (Fig. 31).

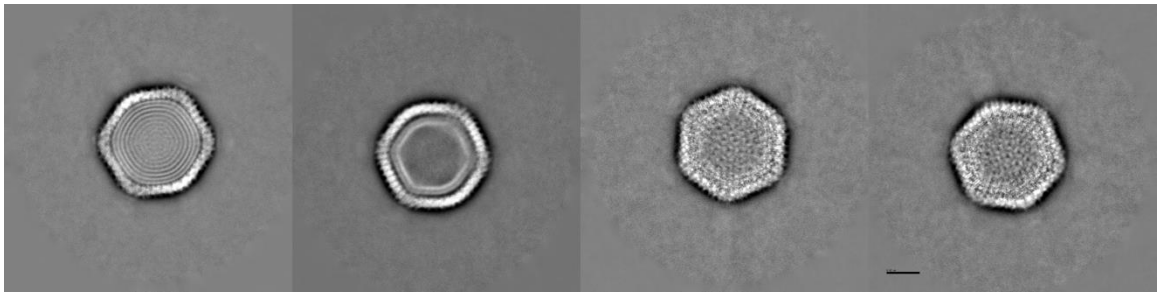

Figure 31. Class Averages of PR772. Scale bar = 0.2μm

These class averages are slightly different, and it is hypothesized that perhaps all of the particles were in fact damaged or at different stages of "activation", meaning that particles that appeared whole were potentially at an early stage of activation or had not been triggered.

Heterogeneity was also reflected in the preliminary volume analysis (Fig. 32). Some particles were clearly icosahedral, but others exhibited some "rounding". This might be attributed to the swelling of the particles or a result of decreased internal pressure due to damage or release of the viral DNA.

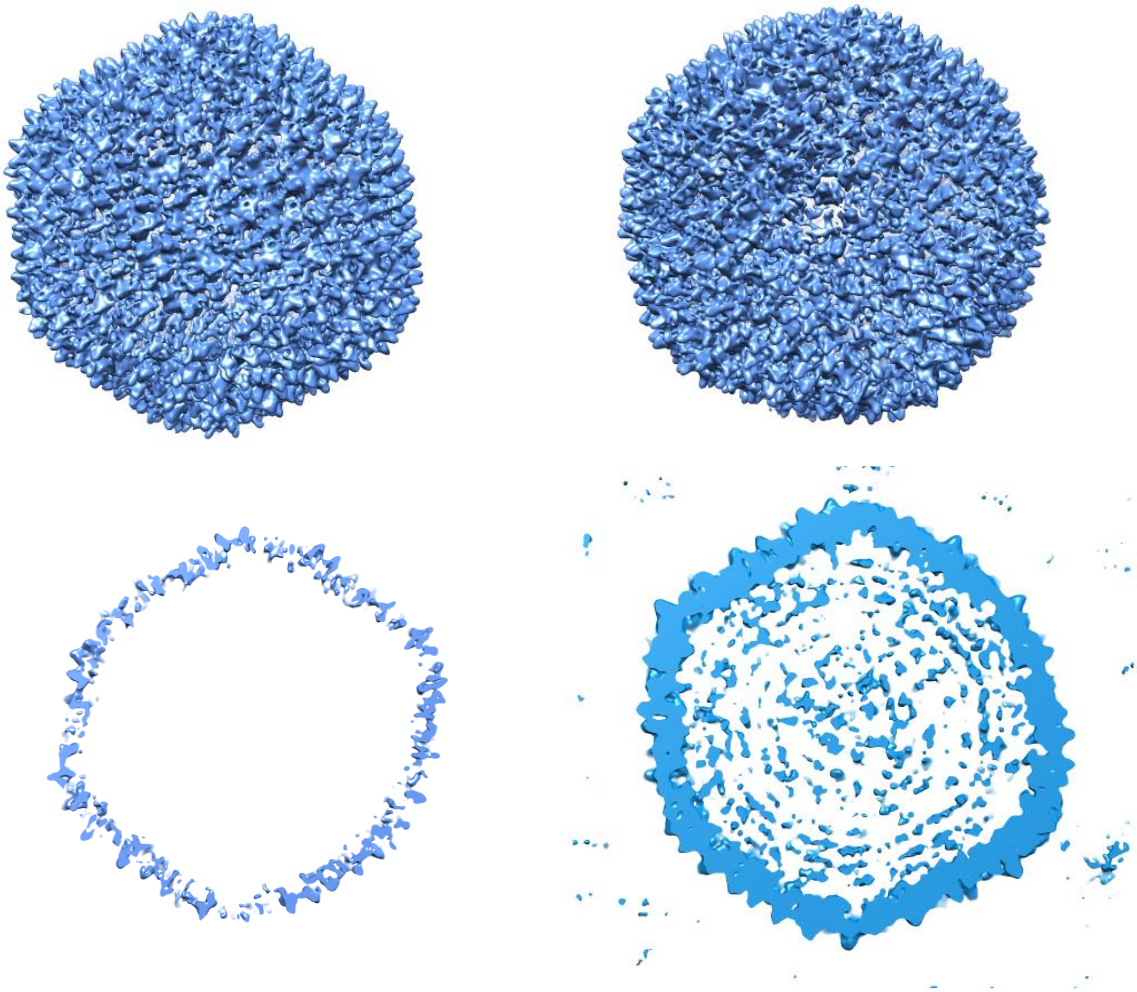

Figure 32. Volume Analysis of PR772 Data Set.

v. CsCl Step Gradient Purification

A CsCl step gradient was implemented as an additional purification step and to further concentrate preparations of PR772 for cryoEM. This was implemented after heterogeneity was still observed with the PR772 sample. The densities used were carefully layered on top of each other in an ultracentrifuge tube. Several 2-month-old

sample preparations were combined and layered on top of the 1.34g/cm^3 density solution. After centrifugation two bands were observed (Fig.33).

Figure 33. Band Formation After CsCl Purification.

The top and bottom bands were both extracted, buffer exchanged and visualized with EM. The particles appeared to be intact, but there were some areas where the virus appeared aggregated and damaged (Fig. 34). It is hypothesized that due to the age of the virus sample that it did not hold up during ultracentrifugation, although those damaged particles should be separated from intact particles.

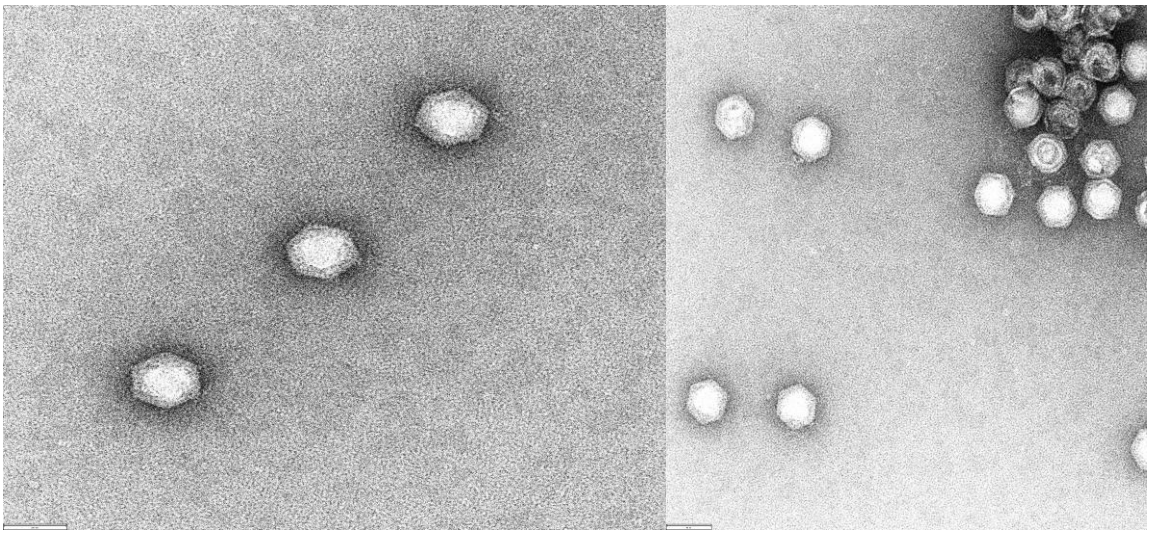

Figure 34. CsCl Purification Resulting PR772 Particles.

A new virus preparation was made and put on a CsCl step gradient made up of 1.7 g/cm^3 and 1.34 g/cm^3 densities. These densities were carefully layered on top of each other in an ultracentrifuge tube with the fresh sample gently layered on top of the 1.34 g/cm^3 CsCl density. Ultracentrifugation was carried out for 4 hours, rather than 2 hours. The time change was implemented to allow for a longer separation time to yield a homogenous virus sample. After 4 hours of centrifugation two bands were present above the 1.34 g/cm^3 CsCl, similar to what was previously observed (Fig 35). These bands were extracted, and 100 μL of the extracted band was buffer exchanged and further diluted 1:10. This dilution was used for negative staining and visualization with EM.

Figure 35. Fresh Prep Band Formation After CsCl Step Gradient

The particles at low and high magnifications appeared to be intact, icosahedral in shape, and high in concentration (Fig. 36). This virus prep was plunge frozen and stored in liquid nitrogen for cryoEM analysis at a later date.

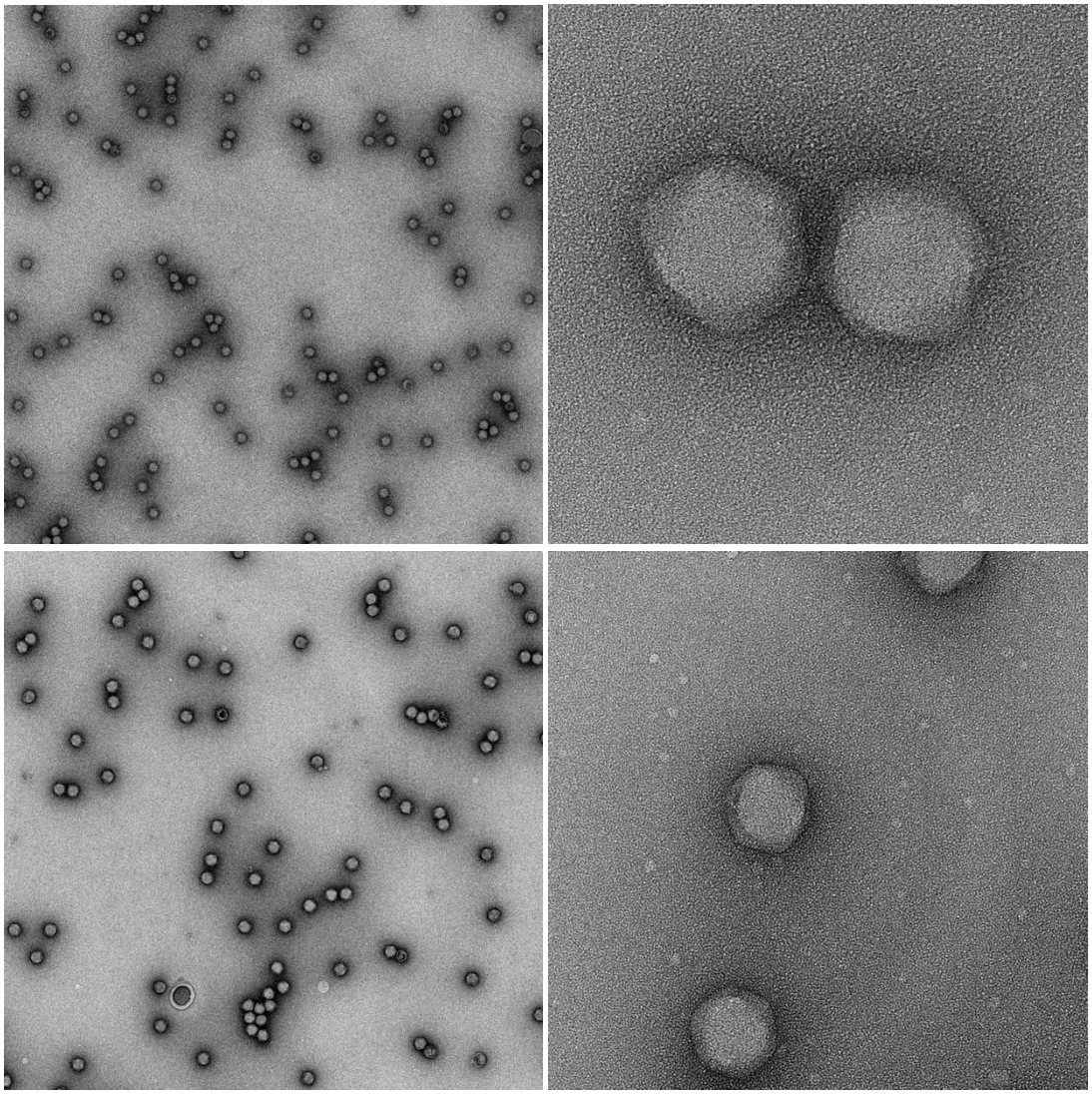

Figure 36. Resulting PR772 Particles After CsCl Step Gradient Purification.

vi. Aging

Previous research showed that "aging" PRD1 allowed for visualization of released lipidic nanotubes (Hong et al.). "Aging" was done by storage of purified virus at 4^{o}C. To determine if "aging" results in PR772 genome release, several virus preps were imaged by negative stain after 1, 2- and 3-months post storage (Fig. 37). Panels A-B are the

images taken at 1 month, panels C-D are images of the 2-month-old prep, and panels E-F are images taken of the prep stored for 3 months (Fig. 37).

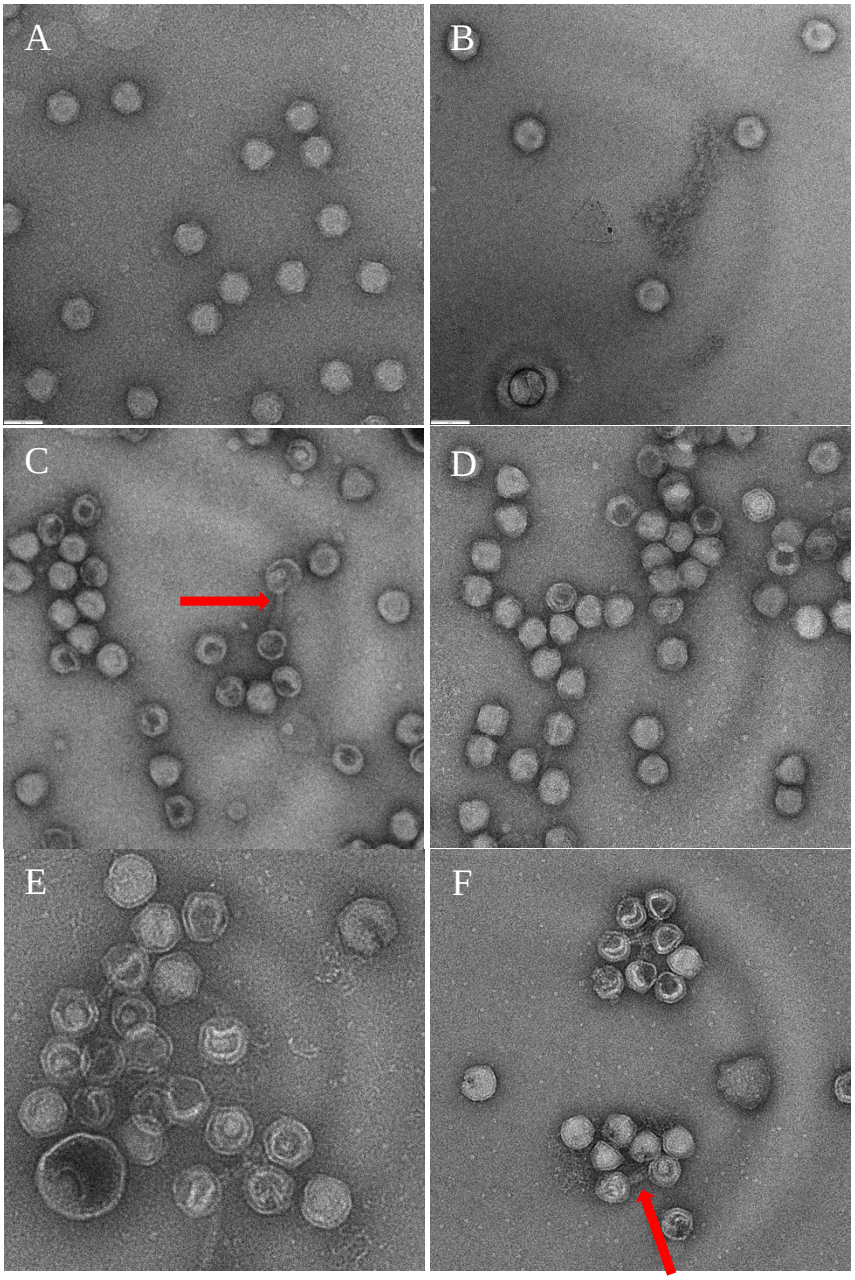

Figure 37. Images of PR772 Particles After Storage for 1 Month (A-B), 2 Months (C-D), and 3 Months (E-F).

Images of each timepoint showed the deterioration of the PR772 particles over time. Although it was previously reported that “aging” would lead to the protrusion of the lipidic nanotube, it appears that the virus is simply degrading over time, with the release of the proteolipidic nanotube and genome content. The formation of the proteolipidic tube can be seen in the preps that were stored for 2-3 months.

CHAPTER 5

DISCUSSION

i. XFEL and Cryo-EM Applicability

Research in structural biology aims to provide understanding of critical biological processes that are involved in a variety of molecules (Cheng). Many of the insights for this come from the structures of molecules and complexes involved in these processes (Cheng). Atomic structures give insight for drug and therapeutic development as it gives information regarding potential targets. Nuclear Magnetic Resonance (NMR) and X-ray crystallography has been the methods generally used for structure discovery and prior to 2013 most of the structures in the protein data bank (PDB) were obtained using these methods (Cheng). Crystallography of virus particles generally requires significant effort to obtain crystals that diffract well. Recent advances in cryoEM for structural studies opened increased opportunities for virus structural studies. XFELs are also becoming a promising alternative for structure reconstruction.

Single particle cryoEM determines structures by combining individual images of molecules that are similar (Cheng). Structure reconstruction by cryoEM has produced high resolutions making it an attractive alternative to X-ray crystallography. Developments in cryoEM including improved microscope optics and controls, detectors, and image analysis software make this instrumentation valuable for structure determination for a variety of macromolecules, including those that undergo conformational changes. Analysis of complexes undergoing conformational changes can be done using multi-conformational reconstruction methods. These developments have

led to structure discovery at higher resolutions than previously reported and insight into macromolecule interactions. In 2015 Sriram Subramaniam and his colleagues reported the structure of a complex between *E. coli*-galactosidase and an inhibitor at the highest reported resolution: 2.2 Å, and in 2018 Kirchdoefer et al. presented the first structures of a trimeric coronavirus spike ectodomain bound to a protein receptor and the first structure of prefusion S1/S2 cleaved coronavirus spikes at a 3.9-4.5 Å resolution (Subramaniam et al.; Kirchdoerfer et al.; Schijven, Sadeghi and Hassanizadeh).

The XFEL is another technique used for structure discovery that allows for "diffraction before destruction", yielding high resolution structures at room temperature of crystallized proteins, and radiation sensitive macromolecules (Johansson et al.). These femtosecond pulses give insight to dynamic information about intermediate states and irreversible reactions (Johansson et al.). The speed of the pulses allows for collection of multiple sets of data during a single beamtime shift. There have been many developments and improvements on several factors that affect data quality and collection. Such developments include detectors with higher dynamic range and faster acquisition rates which provide increased data collection efficiency. Developments made to injectors, crystal delivery media, and fixed target devices has reduced the amount of sample needed for structure determination. Furthermore, data processing software has improved data quality and reduced the amount of data needed. XFELs begin to diminish the boundaries between crystallographic studies and single-molecule structure determination which bypasses crystallization (Johansson et al.).

The XFEL and cryoEM techniques offer the ability to solve structures of single particles at very high resolutions. CryoEM does not require as large of a sample size as the XFEL. CryoEM requires a small sample size that is applied to an EM grid forming a layer of homogenous virus. Since the XFEL experiments are run for 12-14 hours shifts at a time with constant sample being injected, it requires a lot of sample. This way during the experiment a constant stream of sample can be delivered. The sample for both techniques is hydrated but for cryoEM the sample is vitrified while the XFEL experiments are conducted at room temperature. Collection of data for the XFEL occurs when the beam makes contact with the single particle at the interaction point. At this point it is not certain at what angles the beam is hitting the particle. However, cryoEM samples are vitrified, meaning that the sample is effectively immobilized. Although the particles are laid on the grid at random orientations the use of cryoEM tomography, allows for a single particle to be analyzed at different orientations. Meaning that the particles is viewed at different angles due to the rotation of the EM sample stage. This allows the scientist to control what angles of the single particle are being imaged. Imaging using the XFEL does not have this feature because the diffraction patterns collected are of many different particles at many different orientations. Data collections for both techniques are automated, and the image processing follows a similar workflow. Both XFEL and cryoEM are semi-automated data collection processes. During XFEL collection some level of monitoring is required during the experiment by the beam scientist in order to ensure that the beam is working correctly. Suboptimal samples for cryoEM results in the user manually picking particles for imaging.

Lastly, the improvements of protocols, instrumentation and data processing present new opportunities to understanding the dynamic nature of viruses and opens new opportunities to study biologically relevant functions that involve conformational changes using XFEL and cryo-EM sources (Johansson et al.). Although there have been extraordinary strides regarding the cryoEM and XFEL technology there is still a major challenge that has to be dealt with. For both cryoEM and XFEL structural studies, resolution is dependent on the quality of the sample.

ii. Protocol Optimization

The resolution that can be acquired from different visualization techniques is contingent on the characteristics of the sample, preparation methods employed, technical specification of the microscope, and the imaging criterion (Glaeser). There are several steps involved in virus sample preparation. One must make sure to use the proper propagation and purification techniques, characterize the sample, which may include using an electron microscope in order to assure that the sample is homogeneous. In order to obtain a high-resolution structure of single particles, a sample has to be prepared that meets several criteria. These include high concentration of particles, homogeneity, high purity, no aggregation, etc. (Thompson et al.). Single particle structure determination consists of imaging and averaging thousands of particles thus having a high concentration homogenous sample is ideal (Thompson et al.).

There are many steps involved in solving a 3D structure utilizing cryoEM and XFEL sources (Fig. 38). At each step of the process there is a choice in the conditions that the sample is being made. The steps begin with the specimen preparation, the

conditions in which it is being propagated, purified, and lastly its storage conditions. At every step of sample preparation there must be optimization, an extra detail that will ensure that the sample is at its best for structure discovery. When preparing sample for

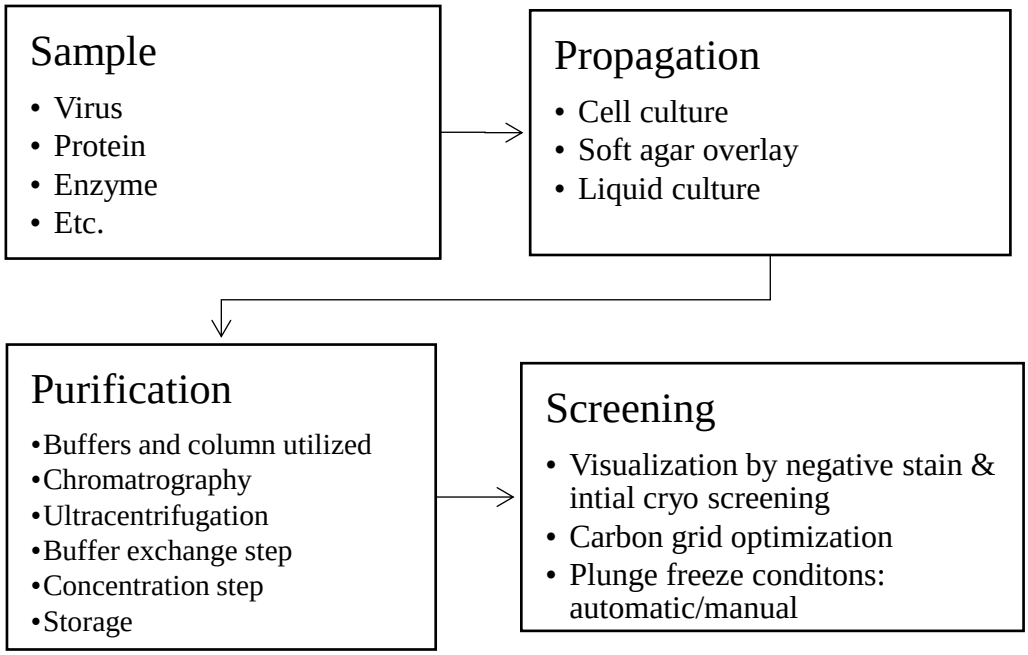

Figure 38. Optimization Workflow for Cryo-EM and XFEL Structural Studies.

structure discovery the conditions at each step of the process must be adequate for virus survival.

A protocol with minimal manipulation of the virus is ideal for viral propagation and purification as it ensures the highest yield of homogenous viral particles. A protocol that requires many steps commonly yields low concentrations of viral particles, given that at each step of the protocol there is potential for loss and damage of viral particles.

Based on the results gathered from my XFEL, and cryo-EM studies, an optimal protocol was developed that yielded a pure, concentrated, homogenous sample. The

protocol was modified from one initially described by Reddy, Hemanth K.N. et al.(Fig. 39) (Reddy et al.).

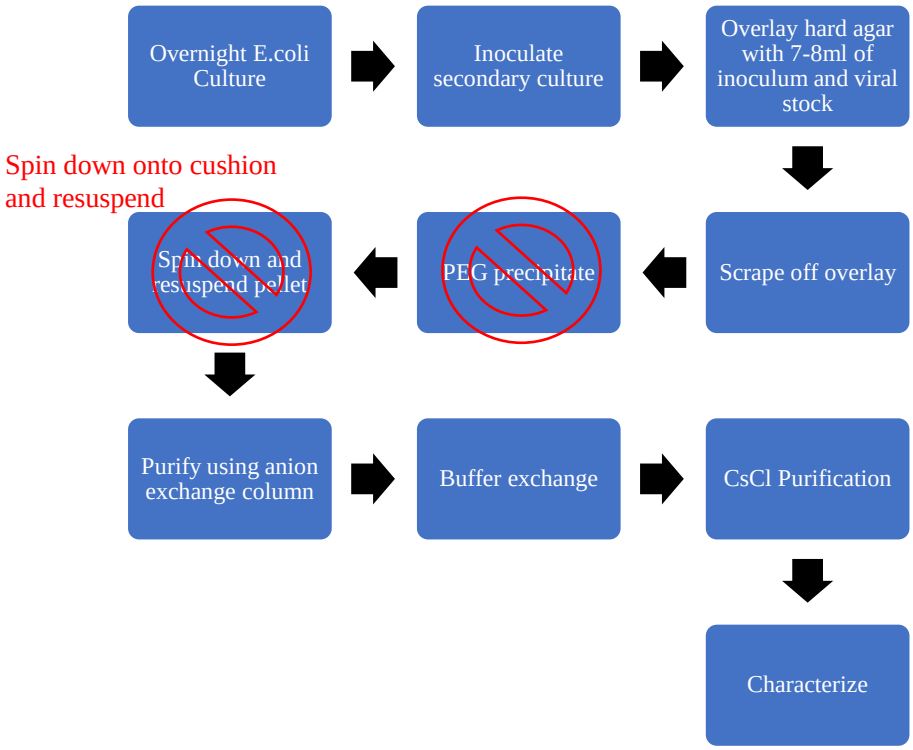

Figure 39. Propagation and Purification Workflow for PR772. Protocol modified from Reddy, Hemanth K.N. et al.

The original protocol included a PEG precipitation step. This step was eliminated due to highly concentrated pili-like structures seen during EM screening. PEG is a hydrophilic molecule with low toxicity that is commonly used as a crowding and concentrating agent. PEG precipitation is a simple, inexpensive technique used to concentrate virus samples (Ingham). Taking into consideration that it is used to concentrate virus particles; it was hypothesized that it would simultaneously concentrate the amount of pili-like structures seen in the sample preparations. EM visualization at low

magnification of PEG precipitated sample preparations revealed that elimination of the step produced virus samples that lacked pili-like structures. A few pili were present, but those were separated from the viral particles using anion exchange chromatography. Visualization of samples after PEG precipitation revealed high aggregation and clustering of virus particles. The virus particles appeared to be stacked on top of each other. The elimination of this step allowed particles to be slightly separated but were still in close proximity to each other. It was hypothesized that PR772 tends to aggregate, but without PEG the particles were observed to not be stacked on top of each other.

Ultracentrifugation, coupled with a cushion or gradient composed of sucrose or CsCl, is commonly used for purification of virus samples. Utilizing a cushion or gradient for ultracentrifugation allows the viral particles to pellet on top of the cushion, rather than the bottom of the tube or in the case of a gradient to sediment according to the density of the particles. This prevents the particles from slamming against the bottom of the centrifuge tube, reducing particle damage. Ultracentrifugation coupled with a cushion was implemented after EM screening revealed damaged particles after ultracentrifugation. 3 mL of 80% sucrose was added to the polypropylene ultracentrifuge tubes to serve as a cushion. Sucrose gradients were previously used for purification, but after EM visualization it was discontinued due to insufficient purity. A cushion with a higher density than the PR772 particles allowed for sedimentation of the virus particles. This change was proven effective by EM analysis, showing that at high magnification the particles appeared intact.

Initial purification was carried out using an anion exchange column attached to a FPLC. The FPLC allows for user manipulation of elution and factors such as pressure. The FPLC system generates reproducible results due its incorporation of automation which includes autosamplers, gradient program control and peak collection (Madadlou, O'Sullivan and Sheehan). Monitoring pressure is important to assure that the appropriate stress is placed on the column for elution without placing too much stress on the column and the virus particles. At ideal pressure levels the amount of damage to virus particles will be minimal. Initial preparations of PR772 without pressure supervision produced broken particles with large amounts of the pili-like structures. It was hypothesized that the particles were broken due to increase in column pressure. Furthermore, the increase in pressure caused the particles attached to the anion resin to shift and elute out ahead of time with impurities. Keeping the pressure between 0.14 - 0.17MPa yielded whole particles and minimal impurities, as confirmed by EM analysis.

An additional purification step was implemented to further purify and concentrate PR772. The CsCl gradient separates particles based on their buoyant density, yielding a highly homogenous virus sample. After purification by anion exchange EM visualization revealed that the virus samples still contained broken and damaged virus particles. Initially several 2-month-old virus samples were purified on a CsCl gradient. Ultimately the final product still had damaged particles, which was attributed to the age of the samples put through the gradient. A fresh virus sample was prepared and purified on a CsCl gradient. EM images revealed that the gradient was able to separate the damaged and intact particles.

Lastly, following the plunge freezing process used for cryoEM sample preparation the PR772 virus particles were observed to be more heterogenous. After PEG concentration, the sample was negative stained and visualized using the EM. The sample appeared pure, and the particles appeared intact. After plunge freezing and imaging several areas on a variety grids on the Krios microscope it became apparent that plunge freezing altered the PR772 virus structure. Lipidic nanotubes were observed and a majority of the particles had expelled their genomic content. Although many particles were triggered, a small subpopulation remained intact. The number of particles that were intact were not enough to yield atomic resolution structural information. For future experiments the plunge freezing process needs to be optimized for PR772. Improvements may include a higher virus concentration, grid preparation, sample application, and blotting.

iii. Structural Studies

The purpose for optimizing the propagation and purification process of PR772 was to achieve a highly concentrated, homogenous sample to determine a high-resolution structure with cryoEM and XFEL.

The X341 beamtime generated approximately 50,000 hits, of which approximately 1,393 were single hits. Ultimately 197, 667 patterns were processed (SPI unpublished preliminary analysis). The highest resolution achieved for PR772 in the previous SPI beamtimes was 9 nm. Initial data analysis for X341 indicates that some diffraction patterns extended to 7 nm in resolution. Unfortunately, there are not enough snapshots at the higher resolution to generate a 3D structure. Since data was collected for

PR772 during several beamtimes, diffraction patterns will be combined to provide a larger dataset that may allow for the reconstruction of a higher 3D structure of PR772. During the analysis, the team might consider, once again removing the icosahedral restriction, to determine if the lipidic nanotube is present on some particles. This would further solidify our initial claim that PR772 has a nanotube that forms from one vertex similar to PRD1.

As a complementary approach, PR772 preps were also imaged by cryoEM. Negative staining and preliminary analysis of the particles allowed for the observation of a nanotube. Many particles after the plunge freezing appeared to have been "triggered" causing the extrusion of the lipidic nanotube. Imaging and data processing for PR772 through this technique was done by Dewight Williams of the John M. Cowley Center for High Resolution Electron Microscopy (CHREM). Heterogeneity was observed in the preliminary volume analysis, some particles were icosahedral, while others exhibited "rounding". This may be attributed to the swelling of the particles as a result of damage or release of the viral DNA. Although the particles were damaged, particles were manually selected and processed to yield a 3D reconstruction at a resolution of 11Å. The resolution achieved was not as high as other structures achieved by this method, but this was attributed to the fact that the sample was suboptimal due to the "triggering" of PR772 during the plunge freezing process.

Nanotubes were observed in "aged" sample preparations. Imaging by negative staining of preps held at 4°C for several months showed that gradual deterioration of the PR772 particle led to the extrusion of the lipidic nanotube. This confirmed that PR772

appears to behave similarly to PRD1 in that “triggering”, caused by infection, environmental changes, or other conditions causes reorganization of the internal membrane.

iv. Applicability of Membrane-Containing Phages

Research of membrane containing phages shows that they are abundant in nature and infect a variety of hosts. Many of these hosts cause illness in plants, animals, and humans. This shows that membrane containing phages have a potential for being used as biocontrol agents (Mäntynen et al.). Examples of this include cystoviruses that have been suggested to be used against bacterial infections of agricultural plants, and PRD1 which has the potential to restrict the horizontal spread of antibiotic resistance genes (Yang et al.). PRD1 infects bacteria that contains conjugative plasmids, which are circular DNA molecules with genes that contain resistance determinants (Ojala, Laitalainen and Jalasvuori). Additionally, phage phi6 has several life science applications. The replication systems based on phi6 polymerase complex or RdRp permit the production of dsRNA molecules that are utilized against plant and human pathogens or to generate an immune response in human cell lines (Mäntynen et al.). Future research will provide insights into a variety of processes of membrane containing phages, leading to a greater understanding of this group of viruses, ultimately offering new applications. Such applications include sources of novel enzymes for biotechnological applications, and insight into the physical properties of the membrane containing viruses to be applied to the engineering of tough composite nanomaterials that are suitable for protection of fragile cargos (Mäntynen et al.; Azinas et al.).

Structure determines function; thus, structure determination is key for insights into a variety of processes that occur within a virus. CryoEM and XFELs present significant new opportunities to understand the dynamic nature of viruses by studying biologically relevant functions and processes that involve conformational changes. CryoEM already provides opportunities to obtain very high-resolution structures of viruses. Single particle structural studies with XFELs is still a developing technology, but recent single particle virus imaging at the European XFEL was very promising. The expectation is that future XFEL virus structural studies will provide significant opportunities to study viruses at high-resolution, room temperature and allow for time resolved studies with a new window for viewing virus functions. CryoEM and XFELs will provide powerful complementary approaches for structural studies. This will expand capabilities for vaccine and therapeutic developments and validation.

REFERENCES

"Challenges for CryoEM." *Nature Methods* 15.12 (2018): 985-85. Print.

"Family - Tectiviridae." *Virus Taxonomy*. Eds. King, Andrew M. Q., et al. San Diego: Elsevier, 2012. 317-21. Print.

Abrescia, Nicola G. A., et al. "Insights into Assembly from Structural Analysis of Bacteriophage PRD1." *Nature* 432.7013 (2004): 68-74. Print.

Ahi, Yadvinder S., and Suresh K. Mittal. "Components of Adenovirus Genome Packaging." *Frontiers in Microbiology* 7 (2016): 1503-03. Print.

Alberts B, Johnson A, Lewis J, et al. *Molecular Biology of the Cell: The Structure and Function of DNA*. 4th Ed: New York: Garland Science, 2002. Print.

Andreasson, Jakob, et al. "Automated Identification and Classification of Single Particle Serial Femtosecond X-Ray Diffraction Data." *Optics Express* 22.3 (2014): 2497-510. Print.

Aquila, A., et al. "The Linac Coherent Light Source Single Particle Imaging Road Map." *Structural Dynamics* 2.4 (2015): 041701. Print.

Azinas, S., et al. "Membrane-Containing Virus Particles Exhibit the Mechanics of A Composite Material for Genome Protection." *Nanoscale* 10.16 (2018): 7769-79. Print.

Baer, Alan, and Kylene Kehn-Hall. "Viral Concentration Determination Through Plaque Assays: Using Traditional and Novel Overlay Systems." *JoVE (Journal of Visualized Experiments)*.93 (2014): e52065. Print.

Calvey, George D., et al. "Mixing Injector Enables Time-Resolved Crystallography with High Hit Rate at X-Ray Free Electron Lasers." *Structural Dynamics* 3.5 (2016): 054301. Print.

Caroline, Ritchie. "Protein Purification." Material and Methods, 2018. Print.

Catalano, C. E. "The Terminase Enzyme from Bacteriophage Lambda: A DNA-Packaging Machine." *Cellular and Molecular Life Sciences CMLS* 57.1 (2000): 128-48. Print.

Catalano, Carlos E., David Cue, and Michael Feiss. "Virus DNA Packaging: The Strategy Used by Phage Λ." *Molecular Microbiology* 16.6 (1995): 1075-86. Print.

Cepko, Constance L., and Phillip A. Sharp. "Assembly of Adenovirus Major Capsid Protein Is Mediated by a Nonvirion Protein." *Cell* 31.2, Part 1 (1982): 407-15. Print.

Chaudhry, Raheel. "Biochemistry, DNA Replication." Ed. Khaddour, Karam. Treasure Island (FL): StatPearls Publishing, 2019. Print.

Cheng, Yifan. "Single-Particle Cryo-EM at Crystallographic Resolution." *Cell* 161.3 (2015): 450-57. Print.

Cockburn, Joseph J. B., et al. "Membrane Structure and Interactions with Protein and DNA in Bacteriophage PRD1." *Nature* 432.7013 (2004): 122. Print.

Coetzee, W. F., and P. J. Bekker. "Pilus-Specific, Lipid-Containing Bacteriophages PR4 and PR772: Comparison of Physical Characteristics of Genomes." *Journal of General Virology* 45.1 (1979): 195-200. Print.

Coren, Jonathon S., James C. Pierce, and Nat Sternberg. "Headful Packaging Revisited: The Packaging of More Than One DNA Molecule into a Bacteriophage P1 Head." *Journal of Molecular Biology* 249.1 (1995): 176-84. Print.

De Jong, R. N., L. A. T. Meijer, and P. C. van der Vliet. "DNA Binding Properties of the Adenovirus DNA Replication Priming Protein Ptp." *Nucleic acids research* 31.12 (2003): 3274-86. Print.

Del Solar, Gloria, et al. "Replication and Control of Circular Bacterial Plasmids." *Microbiology and Molecular Biology Reviews* 62.2 (1998): 434. Print.

Emmett, Stevan R., et al. "The Cell Cycle and Virus Infection." *Cell Cycle Control*. Springer, 2005. 197-218. Print.

Fahy, Gregory M., and Brian Wowk. "Principles of Cryopreservation by Vitrification." *Cryopreservation and Freeze-Drying Protocols*. Eds. Wolkers, Willem F. and Harriëtte Oldenhof. New York, NY: Springer New York, 2015. 21-82. Print.

Filipe, Vasco, Andrea Hawe, and Wim Jiskoot. "Critical Evaluation of Nanoparticle Tracking Analysis (NTA) by Nanosight for the Measurement of Nanoparticles and Protein Aggregates." *Pharmaceutical research* 27.5 (2010): 796-810. Print.

Flint, Jane, et al. *Principles of Virology, Fourth Edition, Bundle*. American Society of Microbiology, 2015. Print.

Fu, Xiaofeng, et al. "The Mechanism of DNA Ejection in the Bacillus Anthracis Spore-Binding Phage 8A Revealed by Cryo-Electron Tomography." *Virology* 421.2 (2011): 141-48. Print.

Glaeser, R. M. "Low Temperature Electron Microscopy-Radiation Damage in Crystalline Biological Materials." *JOURNAL OF MICROSCOPY-OXFORD* 12.1 (1971): 133. Print.

Glaeser, Robert M., and Richard J. Hall. "Reaching the Information Limit in Cryo-EM of Biological Macromolecules: Experimental Aspects." *Biophysical journal* 100.10 (2011): 2331-37. Print.

Gowen, Brent, et al. "The Tailless Icosahedral Membrane Virus PRD1 Localizes the Proteins Involved in Genome Packaging and Injection at a Unique Vertex." *Journal of Virology* 77.14 (2003): 7863. Print.

Grahn, A. Marika, et al. "PRD1: Dissecting the Genome, Structure, and Entry." *The Bacteriophages* (2006): 176-85. Print.

Grant, T., A. Rohou, and N. Grigorieff. "CisTEM, User-Friendly Software for Single-Particle Image Processing." *eLife* 7 (2018): e35383-e83. Print.

Henderson, R., and P. N. T. Unwin. "Three-Dimensional Model of Purple Membrane Obtained by Electron Microscopy." *Nature* 257.5521 (1975): 28-32. Print.

Hockett, K. L., and D. A. Baltrus. "Use of the Soft-Agar Overlay Technique to Screen for Bacterially Produced Inhibitory Compounds." *Jove-Journal of Visualized Experiments*.119 (2017). Print.

Hogue, B. G., and C. E. Machamer. "Nidoviruses." Washington, DC: ASM Press, 2008. Print.

Hong, Chuan, et al. "A Structural Model of the Genome Packaging Process in a Membrane-Containing Double Stranded DNA Virus." *PLoS biology* 12.12 (2014): e1002024. Print.

Hosseinizadeh, Ahmad, et al. "Conformational Landscape Of A Virus by Single-Particle X-Ray Scattering." *Nature Methods* 14.9 (2017): 877. Print.

Hu, Bo, et al. "The Bacteriophage T7 Virion Undergoes Extensive Structural Remodeling During Infection." *Science* 339.6119 (2013): 576-79. Print.

Ingham, Kenneth C. "[20] Protein Precipitation With Polyethylene Glycol." *Methods in Enzymology*. Vol. 104: Academic Press, 1984. 351-56. Print.

Jalasvuori, Matti, and Katariina Koskinen. "Extending The Hosts Of Tectiviridae into Four Additional Genera of Gram-Positive Bacteria and More Diverse Bacillus Species." *Virology* 518 (2018): 136-42. Print.

Johansson, Linda C., et al. "A Bright Future for Serial Femtosecond Crystallography with XFELs." *Trends in Biochemical Sciences* 42.9 (2017): 749-62. Print.

Karhu, Nelli J., et al. "Efficient DNA Packaging Of Bacteriophage PRD1 Requires the Unique Vertex Protein P6." *Journal of Virology* 81.6 (2007): 2970. Print.

Kirchdoerfer, Robert N., et al. "Stabilized Coronavirus Spikes Are Resistant To Conformational Changes Induced by Receptor Recognition or Proteolysis." *Scientific Reports* 8.1 (2018): 15701. Print.

Koning, Roman I. "Chapter 24 - Cryo-Electron Tomography Of Cellular Microtubules." *Methods In Cell Biology*. Eds. Cassimeris, Lynne and Phong Tran. Vol. 97: Academic Press, 2010. 455-73. Print.

Kudryashev, Mikhail, et al. "Evidence of Direct Cell–Cell Fusion In Borrelia by Cryogenic Electron Tomography." *Cellular Microbiology* 13.5 (2011): 731-41. Print.

Langston, Lance D., and Mike O'Donnell. "DNA Replication: Keep Moving and Don't Mind The Gap." *Molecular Cell* 23.2 (2006): 155-60. Print.

Lech, Karen, K. J. Reddy, and L. A. Sherman. "Current Protocols in Molecular Biology." (2001): 1.13.1-1.13.10. Print.

Leiman, Petr G., et al. "Three-Dimensional Rearrangement of Proteins In The Tail of Bacteriophage T4 on Infection of Its Host." *Cell* 118.4 (2004): 419-29. Print.

Liu, Haiguang, and John C. H. Spence. "XFEL Data Analysis For Structural Biology." *Quantitative Biology* 4.3 (2016): 159-76. Print.

Lute, Scott, et al. "Characterization of Coliphage PR772 and Evaluation of Its Use for Virus Filter Performance Testing." *Applied and Environmental Microbiology* 70.8 (2004): 4864-71. Print.

Madadlou, Ashkan, Siobhan O'Sullivan, and David Sheehan. "Fast Protein Liquid Chromatography." *Protein Chromatography*. Springer, 2011. 439-47. Print.

Manns, Joanne M. "SDS-Polyacrylamide Gel Electrophoresis (SDS-Page) of Proteins." *Current Protocols in Microbiology* 22.1 (2011): A-3M. Print.

Meister, Annette, and Alfred Blume. "(Cryo)Transmission Electron Microscopy of Phospholipid Model Membranes Interacting with Amphiphilic and Polyphilic Molecules." *Polymers* 9.10 (2017): 521. Print.

Milne, Jacqueline L. S., et al. "Cryo-Electron Microscopy–a Primer for the Non-Microscopist." *The FEBS journal* 280.1 (2013): 28-45. Print.

Molineux, Ian J., and Debabrata Panja. "Popping the Cork: Mechanisms of Phage Genome Ejection." *Nature Reviews Microbiology* 11.3 (2013): 194. Print.

Mäntynen, Sari, et al. "Half a Century of Research on Membrane-Containing Bacteriophages: Bringing New Concepts to Modern Virology." *Viruses* 11.1 (2019): 76. Print.

Nasukawa, Tadahiro, et al. "Virus Purification by CsCl Density Gradient Using General Centrifugation." *Archives of Virology* 162.11 (2017): 3523-28. Print.

Newcomb, W. W., et al. "The Ul6 Gene Product Forms the Portal for Entry of DNA into the Herpes Simplex Virus Capsid." *Journal of virology* 75.22 (2001): 10923-32. Print.

Ojala, Ville, Jarkko Laitalainen, and Matti Jalasvuori. "Fight Evolution with Evolution: Plasmid-Dependent Phages with a Wide Host Range Prevent the Spread of Antibiotic Resistance." *Evolutionary applications* 6.6 (2013): 925-32. Print.

Panalytical, Malvern. "Nanoparticle Tracking Analysis (NTA) Measurements." 2019. Print.

Peralta, Bibiana, et al. "Mechanism of Membranous Tunnelling Nanotube Formation in Viral Genome Delivery." *PLoS biology* 11.9 (2013): e1001667. Print.

Poon, A. P., and B. Roizman. "Characterization of a Temperature-Sensitive Mutant of the Ul15 Open Reading Frame of Herpes Simplex Virus 1." *Journal of virology* 67.8 (1993): 4497-503. Print.

Prasad, B. V. Venkataram, and Michael F. Schmid. "Principles of Virus Structural Organization." *Advances in Experimental Medicine and Biology* 726 (2012): 17-47. Print.

Rampersad, Sephra, and Paula Tennant. "Chapter 3 - Replication and Expression Strategies of Viruses." *Viruses*. Eds. Tennant, Paula, Gustavo Fermin and Jerome E. Foster: Academic Press, 2018. 55-82. Print.

Reddy, Hemanth K. N., et al. "Coherent Soft X-Ray Diffraction Imaging of Coliphage PR772 at the Linac Coherent Light Source." *Scientific data* 4 (2017): 170079. Print.

Renaud, Jean-Paul, et al. "Cryo-EM in Drug Discovery: Achievements, Limitations and Prospects." *Nature Reviews Drug Discovery* 17 (2018): 471. Print.

Ruch, Travis R., and Carolyn E. Machamer. "The Coronavirus E Protein: Assembly and Beyond." *Viruses* 4.3 (2012): 363-82. Print.

Rydman, Pia S., and Dennis H. Bamford. "Identification and Mutational Analysis of Bacteriophage PRD1 Holin Protein P35." *Journal of Bacteriology* 185.13 (2003): 3795-803. Print.

Santos-Pérez, Isaac, et al. "Membrane-Assisted Viral DNA Ejection." *Biochimica et Biophysica Acta (BBA) - General Subjects* 1861.3 (2017): 664-72. Print.

Saren, Ari-Matti, et al. "A Snapshot of Viral Evolution from Genome Analysis of the Tectiviridae Family." *Journal of Molecular Biology* 350.3 (2005): 427-40. Print.

Schijven, Jack F., Gholamreza Sadeghi, and S. Majid Hassanizadeh. "Long-Term Inactivation of Bacteriophage PRD1 as a Function of Temperature, pH, Sodium and Calcium Concentration." *Water Research* 103 (2016): 66-73. Print.

Strömsten, Nelli J., Dennis H. Bamford, and Jaana K. H. Bamford. "In Vitro DNA Packaging of PRD1: A Common Mechanism for Internal-Membrane Viruses." *Journal of Molecular Biology* 348.3 (2005): 617-29. Print.

Subramaniam, Sriram, et al. "Electron Tomography of Viruses." *Current Opinion in Structural Biology* 17.5 (2007): 596-602. Print.

Sun, Siyang, Venigalla B. Rao, and Michael G. Rossmann. "Genome Packaging in Viruses." *Current Opinion in Structural Biology* 20.1 (2010): 114-20. Print.

Thompson, Rebecca F., et al. "An Introduction to Sample Preparation and Imaging by Cryo-Electron Microscopy for Structural Biology." *Methods* 100 (2016): 3-15. Print.

Thorley, Jennifer A., Jane A. McKeating, and Joshua Zachary Rappoport. "Mechanisms of Viral Entry: Sneaking in the Front Door." *Protoplasma* 244.1-4 (2010): 15-24. Print.

Vestad, Beate, et al. "Size and Concentration Analyses of Extracellular Vesicles by Nanoparticle Tracking Analysis: A Variation Study." *Journal of Extracellular Vesicles* 6.1 (2017): 1344087. Print.

Vénien-Bryan, Catherine, et al. "Cryo-Electron Microscopy and X-Ray Crystallography: Complementary Approaches to Structural Biology and Drug Discovery." *Acta Crystallographica Section F: Structural Biology Communications* 73.4 (2017): 174-83. Print.

Yang, Yuhui, et al. "Characterization of the First Double-Stranded RNA Bacteriophage Infecting Pseudomonas Aeruginosa." *Scientific Reports* 6 (2016): 38795. Print.

APPENDIX A

PERMISSIONS FOR COPYRIGHTED MATERIAL USAGE

SPRINGER NATURE LICENSE
TERMS AND CONDITIONS

Nov 09, 2019

This Agreement between Ms. Alice Contreras ("You") and Springer Nature ("Springer Nature") consists of your license details and the terms and conditions provided by Springer Nature and Copyright Clearance Center.

License Number	4624511021797
License date	Jul 08, 2019
Licensed Content Publisher	Springer Nature
Licensed Content Publication	Nature Methods
Licensed Content Title	Conformational landscape of a virus by single-particle X-ray scattering
Licensed Content Author	Ahmad Hosseinizadeh, Ghoncheh Mashayekhi, Jeremy Copperman, Peter Schwander, Ali Dashti et al.
Licensed Content Date	Aug 14, 2017
Licensed Content Volume	14
Licensed Content Issue	9

SPRINGER NATURE LICENSE
TERMS AND CONDITIONS

Nov 10, 2019

This Agreement between Ms. Alice Contreras ("You") and Springer Nature ("Springer Nature") consists of your license details and the terms and conditions provided by Springer Nature and Copyright Clearance Center.

License Number	4625420653258
License date	Jul 10, 2019
Licensed Content Publisher	Springer Nature
Licensed Content Publication	Nature
Licensed Content Title	Membrane structure and interactions with protein and DNA in bacteriophage PRD1
Licensed Content Author	Joseph J. B. Cockburn et al
Licensed Content Date	Nov 4, 2004
Type of Use	Thesis/Dissertation
Requestor type	academic/university or research institute
Format	electronic

ELSEVIER LICENSE
TERMS AND CONDITIONS

Nov 10, 2019

This Agreement between Ms. Alice Contreras ("You") and Elsevier ("Elsevier") consists of your license details and the terms and conditions provided by Elsevier and Copyright Clearance Center.

License Number	4626560656320
License date	Jul 12, 2019
Licensed Content Publisher	Elsevier
Licensed Content Publication	Current Opinion in Virology
Licensed Content Title	Virus particle dynamics derived from CryoEM studies
Licensed Content Author	Peter C Doerschuk,Yunye Gong,Nan Xu,Tatiana Domitrovic,John E Johnson
Licensed Content Date	Jun 1, 2016
Licensed Content Volume	18
Licensed Content Issue	n/a
Licensed Content Pages	7
Start Page	57